Cyclodextrin nanosponges as adsorbent material to remove hazardous pollutants from water: The case of ciprofloxacin

DOI: 10.1016/j.cej.2021.128514

Cyclodextrin Nanosponges as adsorbent material to remove hazardous pollutants from water: the case of Ciprofloxacin

Vito Rizzi[a], Jennifer Gubitosa[a], Rahel Signorile[a], Paola Fini[b], Claudio Cecone,[c] Adrián Matencio,[c] Francesco Trotta,[c] Pinalysa Cosma[a,b*]

[a]Università degli Studi "Aldo Moro" di Bari, Dipartimento di Chimica, Via Orabona, 4- 70126 Bari, Italy;

[b]Consiglio Nazionale delle Ricerche CNR-IPCF, UOS Bari, Via Orabona, 4- 70126 Bari, Italy;

[c]Dipartimento di Chimica –Università di Torino - Via Pietro Giuria 7 – 10125 Torino

*Prof. Pinalysa COSMA

Università degli Studi "Aldo Moro" di Bari

Dipartimento di Chimica

Via Orabona, 4

I-70126 Bari, ITALY

e-mail: pinalysa.cosma@uniba.it

tel. +39 0805443443

fax +39 0805442128

ABSTRACT

This study was developed inside the European Project Life “Clean up” (LIFE 16 ENV/ES/000169) to search suitable adsorbents to purify treated water from emerging pollutants. Particularly, among pollutants, the attention was focused on Ciprofloxacin removal, a largely used antibiotic, and, for the purpose, Cyclodextrin-based nanosponges were selected, characterized, by using FTIR-ATR, DSC, TG, SEM and XRD analyses, and proposed as recyclable adsorbent. Indeed, the *in-batch* adsorption process was quite complete removing, in a few minutes, 90 % of the pollutant from water, with a maximum adsorption capacity of 2 mg/g. A better comprehension of the adsorption mechanism was obtained by studying the effect of various experimental parameters on the process, *i.e.* ionic strength, pH values, adsorbent/pollutant ratio, and temperature values. The thermodynamics ($\Delta G°<0$ $\Delta H°<0$ and $\Delta S°>0$), the adsorption isotherms (Langmuir, Freundlich, Temkin, and Dubinin–Radushkevich) and kinetics of the process were also investigated. In particular, the applicability of all the proposed isotherms, with exception of the Langmuir model, was observed, and the finding highlighted the heterogeneous character of the adsorption process. The pseudo-second-order kinetic model well described the process and the application of the Weber-Morris model suggested that the adsorption was constituted by two main consecutive steps. Despite the relatively low adsorption capacity, desorption experiments, recycling the 80% of the pollutant for each cycle, were performed and for the purpose 0.1M NaCl was used, lowering the environmental impact. It should be mentioned that, if on one hand the use of salt, to desorb the pollutant, affected the morphological and thermal features of the adsorbent, on the other hand, it did not alter largely the polymer adsorption capacity favoring the Ciprofloxacin removal for several cycles of adsorption and desorption. Moreover, other pollutants, such as Diclofenac, Carbendazim, Furosemide, and Sulfamethoxazole were successfully removed from water, also if present in a quaternary mixture, opening the possibility to use this adsorbent for real water treatments.

KEYWORDS: Cyclodextrins polymers; Emerging pollutants; Ciprofloxacin; Adsorption; Green Chemistry; Recycling

1. INTRODUCTION

Water is essential for human life and its reuse represents an important worldwide challenge. Not surprisingly, scientific research, to ensure its safety and quality, continuously tries solutions to obtain clean water.[1,2] RIF VERDI For years, the removal of many substances from water has been taken into considerations, and, among pollutants, the attention, in the past, was mainly devoted to textile dyes and heavy metals.[3–8] However, unregulated and hazardous chemicals, known as Emerging Contaminants (ECs), have been highlighted as an important and worldwide environmental alarm, and their removal must be taken into account.[1,2,9–11] Pesticides, herbicides, insecticides, fungicides, pharmaceutical compounds, personal care products, etc are considered ECs that, with their metabolites, are continuously introduced into the aquatic environment.[1,2,9–11] With particular reference to pharmaceutical compounds, as main group of ECs, there are the largely used antibiotics both for animal and human medicine.[12] This class of molecules, poured into water, can favor antibiotic resistance causing other important health problems for humans. [13–15] Among these drugs, it is worth to mention Ciprofloxacin (CIP), a third-generation fluorinated quinolone-based compound, that is one the most used thanks to its great stability and effective broad-spectrum antimicrobial activity.[13] As reported in the literature, the presence of CIP in water, wastewater, and

effluents from hospitals has been observed in a concentration range from 150 μg/L (in wastewater from hospitals) up to 31 mg/L (wastewater from drug production facilities).[14–16] Additionally, the presence of CIP unmetabolized residues, coming from animal feces and urine pathways, can cause severe adverse effects on human health disturbing as a whole the natural ecosystems.[17,18]

Due to all these negative effects, the CIP removal from water is an object of study. For this purpose Khan *et al*.[16] described the use of several techniques, used for ECs removal from water.[16] However, the simplicity, cheapness, and efficiency associated with the adsorption technology makes it one of the most effective methods for CIP removal from water.[18] Further, the use of adsorption processes is still preferred in this field because it is considered a hazardous by-product-free operation with a positive environmental impact.[1,2,17,18,9–16] Accordingly, many papers have been reported in the past and recent literature.[12,13,22–26,14–21] In particular, **Table 1** reports the most recent and interesting works available in the literature showing the different classes of used adsorbents. More importantly, by considering the number of works available in 2020, [12,13,16,21,23] active research is still in course, demonstrating that important advances in this field should be expected by the scientific community. The challenge is to find sustainable, low cost and efficient processes with the important feasibility of recycling both the adsorbent and the pollutant according to the principles of "Green Chemistry" and "Green Economy".

About this purpose, it should be mentioned that the most part of adsorbents reported in **Table 1** work well (with very high q_{max} values) however, only in the few cases [inserire 12, 16, e range 23-26], the reuse of the material was successfully achieved by using unsafe, environmentally unsustainable approaches (as will be discussed later along the paper) or relatively long contact times. On this basis, intending to propose at same time a more safety and very performant adsorbent for potential industrial applications, this work reports the use of a Cyclodextrins-based polymer, cross-linked with 1-4 butanediol diglycidyl ether. More specifically, recyclable nanosponges are proposed for CIP removal and recovery from water by adopting an environmental friendly approach. So, novel

cross-linked polymeric structures characterized by a three-dimensional network, with a crystalline and amorphous structure, spherical shape, and good swelling properties, are presented,[27] by underlining their wide potential and very low toxicity.[28–31] Not surprisingly, the cross-linking of Cyclodextrins with epichlorohydrin was largely investigated in the past, but it has been reported that epichlorohydrin is highly toxic for humans and animals.[26] Moreover, with respect the papers reported in **Table 1**, the present work proposes not only the fast CIP removal from water but also the use of diluted 0.1 NaCl solutions to enable the easy and fast adsorbent regeneration obtaining the quite complete CIP recovery. As result, the use of hard conditions of work or organic solvents is thus avoided according to "Green Chemistry" principles. Indeed, numerous adsorption/desorption cycles were also studied avoiding the disposal of the adsorbent as secondary hazardous waste material. Despite the use of salt, to desorb the pollutant, affected the morphological and thermal features of the adsorbent, it did not alter the polymer adsorption capacity favoring the Ciprofloxacin removal for several cycles of adsorption and desorption. So, the adsorbent lifetime extension was also demonstrated according to the Green Economy requests, overpassing the problem related to the observed polymer low adsorption capacity (q_{max}=2 mg/g) for the CIP. Another important aspect regards the application of the adsorbent to various typologies of pollutants. Effectively, the adsorbents reported in **Table 1** were tested only for the CIP removal, while a suitable material for the industrial-scale application should offer the possibility to remove a larger number of ECs and their families. Accordingly, the proposed adsorbent was tested also with other contaminants, removing in few minutes not only CIP but also different classes of ECs such as drugs and pesticides, *i.e.* Diclofenac, Carbendazim, Furosemide, and Sulfamethoxazole, also in mixture. Additionally, besides the kinetic and the thermodynamic analyses of the adsorption process, preliminary results about the possibilities to work not only *in batch* but also under dynamic conditions (in *flux mode*) are presented, by observing the important absence of counter pressures also for a prolonged adsorbent use. Since this work has been supported by the LIFE+ European Project named LIFE CLEAN UP, also a semi-

industrial prototype has been developed, and work is in progress about the possibility to use this polymer for industrial applications to treat water.

2. MATERIALS AND METHODS

2.1 Materials and methods. β-Cyclodextrins (βCD) were obtained from Roquette Freres (Lestrem, France), α-Cyclodextrins (αCD) and γ-Cyclodextrins (γCD) were purchased from Cyclolab (Budapest, Hungary). α-Cyclodextrins, β-Cyclodextrins, and γ-Cyclodextrins were brought up to constant weight before use in an oven at 75°C. 1,4-Diazabicyclo [2.2.2] octane (DABCO), 1,4 butanediol diglycidyl ether (BDE), and Ciprofloxacin ($C_{17}H_{18}FN_3O_3$, M.W. 331.35 g×mol^{-1}) were purchased from Sigma-Aldrich (Milan, Italy) and used as received. Ciprofloxacin stock solution was prepared at a concentration of 10 mg×L^{-1} and further diluted, with deionized water, according to the case. By using concentrated HCl and NaOH solutions, the pH of the aqueous solution was adjusted, when necessary. Salt stock solutions were prepared and diluted in a Ciprofloxacin one to investigate the ionic strength role. Measurements were executed in triplicate, calculating the corresponding standard deviation.

2.2 Polymer synthesis.

In a typical procedure, the synthesis of the polymer was carried out by dissolving 2.15 g of α-CD, 2.50 β-CD, and 2.85 γ-CD in 10 mL of 0.2M NaOH sodium hydroxide distilled water solution, using a round-bottom flask. Thereafter, while continuously stirring the solution, 0.37 g of DABCO was added. Eventually, 4.85 mL of BDE was added, and the temperature was increased to 90°C, using a hotplate stirrer equipped with thermoregulation and a metal hemispheric bowl to obtain homogeneous heating of the flask. The reaction was then allowed to occur for 90 minutes, ultimately obtaining a monolith block as a product. Later, the product was recovered from the flask by crushing with a spatula and subsequently purified with distilled water, to remove any non-reacted reagents. At the

end of the purification step, the product was dried in an oven at 70°C up to constant weight and ground with a mortar, obtaining a powder.

2.3 UV-Visible measurements. A Varian CARY 5 UV-Vis-NIR spectrophotometer (Varian Inc., now Agilent Technologies Inc., Santa Clara, CA, USA) was employed for registering UV-Vis absorption spectra in a range of 200–800 nm, at a 1nm/s scan rate. The CIP concentration was followed up by evaluating the absorbance intensity at λ=335 nm by using a molar absorption coefficient (ε) of 14200 $L \times mol^{-1} \times cm^{-1}$, experimentally evaluated through the application of the Lambert-Beer law.

2.4. Gas-volumetric analysis. Nitrogen adsorption–desorption isotherms were measured at 77 K using a Micromeritics ASAP2010 volumetric sorption analyzer (Norcross, GA, USA). Before the adsorption measurements, the sample was outgassed at 100 ◦C under vacuum for 15 h to remove the adsorbates and residual moisture. The specific surface area was estimated using the BET equation.

2.5 Scanning Electron Microscopy (SEM) analyses. The morphology and chemical composition of the samples were studied by scanning electron microscopy (SEM). The images were acquired with a FEG-SEM TESCAN S9000G (Brno, Czech Republic) using secondary electrons, 10 kV accelerating voltage, and ultra-high resolution. Before SEM characterization, the samples were ion-coated with 2 nm of chromium, using a sputter coater. Energy Dispersive X-ray (EDX) analysis was also performed.

2.6 X-Ray Diffraction (XRD) analyses. Powder XRD patterns were recorded using a Panalytical X'Pert PRO diffractometer working in Bragg-Brentano geometry and equipped with a Cu-anode X-rays source (λ = 1.541 Å). Data were collected over an angular range from 3 to 70◦2θ at a step size of 0.017 ◦2θ and a time per step of 74.93 s in capillary configuration (capillary diameter = 0.8 mm).

2.7 FTIR-ATR spectroscopy measurements. FTIR-ATR spectra were recorded in a 450–4000 cm^{-1} range, using a Fourier Transform Infrared spectrometer (FTIR Spectrum Two from Perkin Elmer, Waltham, MA, USA), whose resolution was set at 4 cm^{-1}. 16 scans were summed for each acquisition.

2.8 Thermal gravimetric (TG) and Differential Scanning Calorimetry (DSC) analyses. The thermal properties of the polymer were investigated by DSC (Perkin Elmer – DSC 4000) and TG (Perkin Elmer Pyris 1) analyses under a nitrogen flow of 50 mL/min at the heating rate of 10 °C/min. The TG experiments were performed from 30 °C to 600 °C. In the DSC experiments the samples were heated from 20 °C to a maximum temperature of 400 °C .

2.9 *In batch* equilibrium experiments. q_t ($mg \times g^{-1}$) values, *i.e.* the polymer adsorption capacities for CIP, were calculated at varying of the time *t*, by using **Equation 1**:[1,2,9–11]

$$q_t = \frac{C_0 - C_t}{W} \times V \quad \textbf{(1)}$$

where V = CIP solution volume (15 mL), W = dried adsorbent mass (g), C_0 and C_t (mg/L) are the CIP concentration at initial and *t* time, respectively.

To assess the role of CIP amount during the adsorption process, 1 g of the polymer was swelled into vessels with 15 mL of a solution of CIP at diverse initial concentrations (2,5 mg/L, 5 mg/L, and 10 mg/L). The adsorption process was executed under continual stirring at 250 rpm. For evaluating the CIP removal efficiency from water and the adsorbent adsorption capacities UV-Vis absorption spectra were recorded at several contact times. At the same time, the adsorbent amount effect was investigated, and for the purpose, the following amounts were used: 1; 0.5; 0.25; 0.1; 0.05 g by adopting a CIP concentration of 5 mg/L. The solution ionic strength, (by using different salts at several concentrations), changes in pH values (ranging from 2 to 12), and temperature effects on the adsorption process, were also studied. In the latter case, the measurements were performed by using a thermostatic magnetic stirrer hotplate equipped with a thermometer.

2.10 Adsorption kinetics. The kinetic models of pseudo-first-order (PFO) and pseudo-second-order (PSO) were adopted. In particular, the following equations for PFO (**Equation 2**) and PSO (**Equation 3**) models were used:[1,2]

$$ln\,ln\,(q_e - q_t) = ln\,ln\,(q_e) - K_1 \times t \quad \textbf{(2)}$$

$$\frac{t}{q_t} = \frac{1}{K_2 q_e^2} + \frac{1}{q_e} \times t \quad \textbf{(3)}$$

with q_e = polymer adsorption capacities at equilibrium and q_t = the same adsorption capacity at time *t*, both in mg/g. Instead, the rate constants of PFO and PSO models are k_1 (min^{-1}) and k_2 (g/(mg×min)), respectively.

2.11 Thermodynamic studies. The thermodynamic parameters, free energy ($\Delta G°$), entropy ($\Delta S°$), and enthalpy ($\Delta H°$), were inferred for the CIP adsorption on nanosponges at 298, 323, 343 and 363 K.[9–11] The free energy was calculated by using **Equation 4**:

$$\Delta G° = - RT \ln K_{eq} \quad \textbf{(4)}$$

with R = universal gas constant (8.314 $J \times mol^{-1} \times K^{-1}$), T = temperature (K) and K_{eq} = equilibrium constant. The values of $\Delta H°$ and $\Delta S°$ were found by combining **Equations 4** and **5** to obtain **Equation 6.**

$$\Delta G° = \Delta H° - T\Delta S° \quad \textbf{(5)}$$

$$lnK_{eq} = -\frac{\Delta H^0}{RT} + \frac{\Delta S^0}{R} \quad \textbf{(6)}$$

2.12 Adsorption Isotherms. To infer more information about the adsorption process, Langmuir, Freundlich, Temkin, and Dubinin–Radushkevich isotherms were applied to experimental data.[11] In particular, it is well-known that the Langmuir model is based on 3 key points: (a) all sites are characterized by constant adsorption energy, (b) each site is occupied only by one molecule and no interaction between the molecules arises, and finally (c) the adsorption is localized. The linear form of the Langmuir equation is reported as **Equation 7**:

$$\frac{C_e}{q_e} = \frac{1}{K_L Q_0} + \frac{C_e}{Q_0} \quad \textbf{(7)}$$

where q_e = CIP adsorbed amount at equilibrium in mg/g, C_e = CIP equilibrium concentration in solution in mg/L, K_L = Langmuir equilibrium constant (L/mg), and Q_0 = maximum adsorption capacity in mg/g. The model of the Freundlich isotherm, instead, represents a purely empirical approach by describing the adsorbent surface as heterogeneous with adsorption sites having different energies as a function of the surface coverage. The linear form of the Freundlich isotherm equation is displayed in **Equation 8**:

$$lo(q_e) = lo(K_F) + \frac{1}{n} lo(C_e) \quad \textbf{(8)}$$

K_F (L/mg) = the Freundlich constant and n = the heterogeneity factor. K_F is referred to the adsorption capacity, whereas the 1/n value measures if the adsorption process is irreversible (1/n=0), favorable (0<1/n<1), or unfavorable (1/n>1). As for the Temkin model, it gives an idea about the influence of the adsorbate-adsorbent interactions on the adsorption energy. In detail, the Temkin isotherm indicates that, during the adsorption process, the heat of adsorption relative to all the molecules in the coverage diminishes linearly due to adsorbent–adsorbate interactions. Moreover, a uniform

distribution of binding energies characterizes the adsorption. The linearized form of the Temkin model is shown in **Equation 9**:

$$q_e = B_1 ln(K_T) + B_1 ln(C_e) \quad \textbf{(9)}$$

B_1 and K_T are parameters determined from the slope and the intercept by applying **Equation 9**, respectively. K_T corresponds to the equilibrium binding constant in L/mol and represents the maximum binding energy. B_1 refers to the heat of adsorption. Finally, the model of Dubinin–Radushkevich isotherm (D-R) was also applied for describing the adsorption mechanism onto a heterogeneous surface by a Gaussian energy distribution. Once again, the linearized form of the model equation was used and displayed as **Equation 10**:

$$lnq_e = ln(Q_0) - K_{D-R} \times \varepsilon^2 \quad \textbf{(10)}$$

Here q_e (mg/g) represents the equilibrium adsorption capacity, Q_0 (mg/g) is the theoretical capacity of isotherm saturation and $K_{D\text{-}R}$ (mol^2/J^2) is the constant of the Dubinin–Radushkevich isotherm. ε is the potential of Polanyi and it is described by **Equation 11**:

$$\varepsilon = RTln(1 + \frac{1}{C_e}) \quad \textbf{(11)}$$

where R = gas constant (8.314 J/mol K), T = absolute temperature (K), and C_e = adsorbate equilibrium concentration (mg/L).

The model is applied to assess the nature of the adsorption process; it means it distinguishes the physical and chemical adsorption by inferring the value of energy, E, by applying **Equation 12**:

$$E = \frac{1}{\sqrt{2K_{D-R}}} \quad \textbf{(12)}$$

A value of E within the range 8-16 kJ/mol implies the necessity of taking into account the chemisorption as part of the adsorption process, while for E < 8 kJ/mol, the physisorption should be involved.[11]

2.13 *In batch* desorption experiments. For inducing the release of the adsorbed CIP the chosen electrolyte was NaCl, in the optic of improving the eco-sustainability of the process. For the purpose, several concentrations were explored and 0.1 M NaCl was selected as the best one for executing consecutive cycles of adsorption/desorption. Once again, the UV-Vis absorption spectroscopy was used for determining the quantity of the desorbed pollutant. In particular, the loaded adsorbent (from this experimental condition: 15 mL of 5 mg/L CIP on 0.25 g of adsorbent, contact time of 60 minutes) was washed with fresh water (15 mL of water and stirred for 15 minutes) for eliminating the unadsorbed CIP, then swollen in the 15 mL of NaCl solution for the release. The desorption process was monitored at several contact time. In the same way, when the recycle of the adsorbent was evaluated, after each cycle of adsorption/desorption (by using 15 mL of 5 mg/L CIP adsorbed on 1 g of adsorbent), fresh water was used for removing the excess of salt from the adsorbent. In this case, the desorption process was evaluated after 60 minutes, adopted as contact time.

2.14 Determination of zero-point charge of Cyclodextrins based polymer. The pH of zero-point charge (pH_{ZPC}) of nanosponges was measured following the procedure reported by Rizzi *et al*.[10] In detail, the pH drift method was applied. Volumes of 25 mL of 5.0×10^{-2}M NaCl solutions were prepared by regulating the pH values within the range 2 - 12 (pH_i) by means of the addition of HCl and NaOH. Then, the solution pH was measured before (pH_i) and after (pH_F) the swelling of 70 mg

of the adsorbent for 48 h under continuous stirring. The value of pH_{ZPC} is obtained from the intersection of the line of pH_i versus pH_i with the curve pH_i versus pH_F.

3. RESULTS AND DISCUSSION

3.1. Physicochemical features of the polymer. As the first step of this study, the physical and chemical characteristics of the adsorbent material, previous its use for the CIP adsorption, were investigated. So, by using in synergy several complementary techniques, the results reported in the following section were obtained.

3.1.1. SEM and XRD analyses. The used adsorbent was studied by SEM and EDX in order to infer some information about its morphology and chemical composition. Due to the presence of cyclodextrins, adopted as monomers, and the used cross-linker, the EDX analysis indicated the main occurrence of C and O with the following atomic percentages 33.33% and 66.67%, respectively. Interestingly, the SEM images of the unloaded polymer, with different magnification ratios, reported in Fig. 1A-D, suggest the presence of dimensionally polydispersed polymer granules, whose size was roughly comprised between a few tens to two hundred microns. The morphological characterization also revealed smooth external surfaces and the absence of any macro- and mesoporosity. The latter was further studied by gas-volumetric analysis, which confirmed the bulky features of the resulting polymer granules. The specific surface area resulted in roughly 1 m2/g, and the absence of micro-porosity was also observed. Mallard *et al*. [37] reported that the cross-linker's introduction, needed for the polymerization, should reduce the well-known crystallinity of the parent cyclodextrins used as monomers. Accordingly, Fig. 1E shows the XRD pattern of the polymer (black line) with the presence of a single band, denoting that the polymer was amorphous [37].

3.1.2. FTIR-ATR spectroscopy measurements. As expected, during the FTIR-ATR spectroscopy measurements, the typical spectrum of cyclodextrins, reported in Fig. 2A (black line), already carefully described in the literature [38] and obtained for other cross-linked cyclodextrin polymers was observed [37,39]. A large band was detected at 3354 cm□ 1 due to the symmetric and anti-symmetric O–H stretching modes; accordingly, the related OH bending occurred at 1640 cm□ 1. The C–H stretching of cyclodextrins and cross-linker were observed at 2932 and 2869 cm□ 1. The C-O-C or C-O bond vibrations in the hydroxyl groups of cyclodextrins were identified in the region 1080–1000 cm□ 1 [39–41]. At the same wavenumbers, the contribute of the cross-linker should be considered [37]. The bands in the region 950–650 cm□ 1 can be attributed to C–H bonds and glucopyranose cycle vibrations. In details, if at 856 cm□ 1, the C–C–H bending was observed, on the other hand at 750 cm□ 1 and 709 cm□ 1, the C–C-O bending were detected. Moreover, the bands below 900 cm□ 1 were also attributed to the stretching vibrations of the epoxide in the cross-linker [37]. Finally, the region 1400–1150 cm□ 1 reported the absorption bands attributed to C–H bonds deformation ascribed to cyclodextrins primary and secondary hydroxyl groups [39,40].

3.1.4 TG and DSC analyses. More details were obtained by using in synergy TG and DSC analyses. As obtained during the FTIR-ATR investigation, also the TG curve of this polymer (black line) was similar to those of other cross-linked cyclodextrin polymers[42, 43]. In **Figure 2B**, a first stage of decomposition, related to dehydration with a corresponding loss of weight of about 10 % at around 148°C, followed by a second important stage related to the decomposition of the polymer framework with a maximum rate of decomposition at about 355 °C were detected. The latter can be better appreciated by calculating the first derivative of the TG curve (DTG) reported in the *inset* of **Figure 2B**. Actually, the decomposition step started at lower temperatures with a degradation of the crosslinker, and it is followed by the decomposition of the cyclodextrins at higher temperatures; however, the overlapping of these two processes did not allow to examine them separately [44]. The DSC study (**Figure 2C**) of the polymer (black line) confirmed the indications obtained from the TG

analysis. In the same temperature range, where the decrease in weight due to the loss of water was observed, the DSC curve showed a broad endothermic band associated with the water evaporation. At higher temperatures, the presence of a wide exothermic peak with an onset at about 280 °C and a maximum at about 340°C, associated to the decomposition process, was observed. It is worth to mention that the two main weight losses of the polymer, obtained during the TG analyses, occurred at higher temperatures with respect the corresponding parent cyclodextrins, where the water release occurs at temperature lower than 110°C, and the maximum decomposition rate temperatures are 320°C, 328 °C and 324 °C for α-cyclodextrin , β-cyclodextrin and γ-cyclodextrin, respectively [45]. In the cyclodextrin polymer the loss of water was observed at higher temperature since the structure of the polymer is more complex and water can interact not only with cyclodextrins but also with other components of the polymer matrix. The same cyclodextrins are entrapped in the crosslinked network; so, it results in a higher thermal stability of this insoluble polymer than those of the monomeric cyclodextrins.

3.2 The adsorption process: an overview. The typical UV-Vis absorption spectrum of CIP (see the molecular structure in **Figure 3**) presents three maxima at λ=270, 323, and 335 nm, respectively, attributed to π→π* transitions.[31] During this work, these bands were diagnostic to follow the CIP adsorption by using the proposed nanosponges (camera picture in **Figure 3**). For example, **Figure 3** shows the time evolution of the UV-Vis spectra of a 10 mg/L CIP solution in presence of 1 g of adsorbent, and, as can be clearly observed by looking the absorbance bands intensities decreasing, the adsorption process was very fast and complete in the first 15-20 minutes, obtaining the 90% of CIP removal. In particular, to infer the residual CIP amount in water, and thus its adsorbed amount, the Lambert-Beer law was used in conjunction with **Equation 1**, and a q_{max} of 2 mg/g was experimentally obtained.[9–11] So, after these assessments, the effect of several operational parameters that can affect the CIP removal by using CD-based nanosponges, was investigated for better characterizing the process.

3.3 Effect of CIP concentration and nanosponges amount on the adsorption process. As the first step of this study, different amounts of polymer were investigated (**Figure 4A**) and placed inside a 5 mg/L CIP solution at pH 6 and room temperature. By raising the adsorbent amount, from 0.05 g to 1 g, and by adopting for example 30 minutes as contact time, the % of CIP adsorption (**Figure 4A**), increased from 40% to 95%, suggesting the free active sites role of the adsorbent for hosting CIP during the adsorption.[9-11,17] On the other hand, in **Figure 4B**, the influence of the adsorbent amount was extensively studied by calculating the q_t values (**Equation 1**). Although in **Figure 4B** the adsorption capacities decreased at increasing the adsorbent amount, the plateau region beginning (a condition in which the relative maximum adsorption capacity was reached for each process by considering hypothetically that the CIP amount was totally adsorbed) was obtained in the first 10 minutes at the highest polymer amount (1g). So, the finding confirmed that the relative CIP adsorption increased when the ratio CIP/nanosponges was in favor of the adsorbent, as previously observed in **Figure 4A**.[9–11,18]

In accordance with previous literature,[18] for explaining this result it should be considered that, in the presence of large quantities of adsorbent, adsorption sites are not fully saturated during the adsorption process, so the q_t values are reduced even if the removal of CIP appeared quite complete. The role of free active sites can be furthermore evidenced by a closer look at **Figures 4A** and **4B**: when the adsorption process begins, there is a large number of sites for the CIP adsorption, so the q_t values and the % of adsorption rapidly increase; conversely, over time, the free sites for hosting the pollutant decrease reducing the adsorption.[15] Consequently, it is reached a plateau region, where the q_t values and the % of adsorption are leveled off. This finding can be also attributed, as already discussed in similar works,[9,10] to repulsive forces between the adsorbed molecules and those in solution, slowing down over time the diffusion into the adsorbent structure. To better characterize the process, the concentration of CIP, fixing the adsorbent amount at 1 g, was changed as reported in **Figures 4C** and **4D**. Hence, by increasing the CIP quantity in solutions, the % of the pollutant removal

decreased but the adsorption capacities increased. This suggested that the increment of the CIP concentration in solution generated a greater concentration gradient between the aqueous solution and the nanosponges surface, favoring the CIP molecule mass transfer from the solution to the adsorbent, leading to a higher CIP absorption capacity (**Figures 4D**).[25] Moreover, a greater number of collisions between the pollutant, if in high amount, and the adsorbent should be favored enhancing the adsorption (**Figures 4D**).[16] However, the increase in CIP concentration worsened the competition between the contaminant molecules for the limited number of binding sites onto the adsorbent surface, therefore a relatively reduced % of adsorption was observed (**Figures 4C)**.[13] Accordingly, after few minutes, by adopting the smallest CIP amount (**Figure 4D**), it was quickly reached the capacity of maximum adsorption, and the results can be, once again, rationalized considering that the reduction of the ratio CIP/adsorbent enhanced the adsorption, making available more adsorption sites.[1,2] In other words, the results suggested that both the CIP mass transfer and its adsorption on the surface of the polymer, as will be afterward discussed, might have a kinetic relevance during the process according to the condition of work, *i.e.* the CIP concentration, amount of adsorbent and contact time.

After these results, to emphasize the great efficiency of the studied adsorbent, preliminary *in flux* measurements were also considered for a potential scale-up of the process from laboratory to industrial scale. For that purpose, by exploiting a commercial syringe-like column (3.00×5.00 cm), 3 g of adsorbent were put in it and then treated with water for obtaining its swelling. After, a solution of CIP (5 mg/L) was allowed to slowly flow through the column by a piston (see the camera picture reported in **Figure S1**). The eluate was collected and spectroscopically analyzed. **Figure S1** shows the obtained results: after 1 minute of elution, the absorbance of CIP in the related UV-Vis spectrum was completely reduced indicating the important removal of the pollutant also under this condition of work. It is worth mentioning that, the absence of counter pressures was observed when the polymer was blocked inside the syringe-like column also if used for a prolonged time.

3.4 Kinetic analysis: To get more information about the adsorption process dynamic, the kinetics was studied, by applying both the PFO (**Equation 2**) and PSO (**Equation 3**) kinetic models, respectively.[1,2,9–11,15,32] The analysis was obtained by varying both the CIP concentration and the adsorbent amount. The results reported in **Figures S2** were obtained from the q_t values displayed in **Figures 4B** and **4D**. In detail, in **Figures S2A** and **2B**, the PFO model is reported, and it refers to experiments of adsorption performed by changing adsorbent and CIP amounts, respectively. On the other hand, the application of the PSO model, under the same experimental conditions, is showed in **Figures S2C** and **2D**. The corresponding kinetic parameters were inferred and reported in **Tables S1** and **S2**. To select what is the best kinetic model for describing the experimental process, the correlation coefficients R^2, and the comparison between $q_{e,exp}$ (the experimental adsorption capacities at the equilibrium, contact time 60 minutes) and $q_{e,calc}$ (calculated adsorption capacities, obtained by applying the kinetic equations) were evaluated. From **Tables S1** and **S2**, it clearly arises that the R^2 values are better for the PSO model, as well as the comparison $q_{e,exp}/q_{e,calc}$, therefore the PSO kinetic model was considered as the best kinetic pattern. The same behavior was observed by Ashiq *et al.*[15] and Wang *et al*.[33] In particular, Ashiq *et al*.[15] suggested that the CIP removal was controlled by the adsorption mechanism, reporting that the PSO model use implies the occurrence of the CIP surface adsorption through ion exchange mechanism, involving mainly electrostatic interaction, between the substrate and the adsorbate molecules.[15] Additionally, to infer more details, the Weber-Morris model was adopted.[9,10,18,34]

This model is represented by the equation: $q_t = k_{int} \times t^{1/2} + C$, where C = the thickness of the boundary layer and k_{int} = the kinetic constant in $mg/(g \times min^{1/2})$, correlated to the intra-particle diffusion rate. Moreover, it assumes that, if during the process, the only limiting step is the intraparticle diffusion, by plotting q_t values versus $t^{1/2}$, a straight line passing through the origin should be obtained. So, during this work, the model was applied both by adopting different amounts of nanosponges (**Figure S3A**) at constant CIP concentration and different CIP concentrations by fixing the amount of the adsorbent (**Figure S3B**). However, for fitting the experimental data it is necessary to use multiple

linear segments, suggesting that the CIP adsorption process involved more phases, or that other diffusion mechanisms could accompany the intra-particle diffusion.[35] In particular, the use of a small quantity of adsorbent (0.1 and 0.05 g) ensured the Weber Morris model applicability restituting a straight line passing through zero (**Figure S3A**). So, only under the latter condition of work, the rate-limiting step could be considered the intra-particle diffusion due to the reduced number of adsorbent active sites able to host the pollutant. Conversely, in other experimental conditions, two sequential events determined the adsorption process of CIP: during the first period, the key step was the CIP diffusion from the solution to the adsorbent external surface, afterwards, there was the second phase referred to intra-particles adsorption and diffusion.[18] During the second step, since the CIP concentration in solution decreased, and the q_t increased, the adsorption process slowed down, hindering the CIP adsorption, and acquired a kinetic relevance. In accordance with the so far discussed role of active sites, this second step was less evident in presence of CIP 10 mg/L.

3.5 Thermodynamic analysis. Different temperature values were explored for studying the CIP adsorption process of Ciprofloxacin, by using 0.25 g of adsorbent and a CIP solution 5 mg/L solution at pH 6. The results, in terms of % of pollutant removal and q_t, are reported in **Figures 5A and 5B**, respectively.

By observing data in **Figure 5A**, it is evident how the adsorption of CIP increased at increasing the temperature values, suggesting the endothermic character of the process.[10] Further, another reason could be the increment of the diffusion rate of CIP on nanosponges;[16] effect more evident especially at the beginning of the process when more free active sites are available to host the pollutant according to kinetic considerations. The K_{eq} values were determined at each temperature value for inferring the thermodynamic parameters of the process, used in **Equations 4** and **5**, for calculating the corresponding $\Delta G°$ values (**Table S3**).

The spontaneity of the process was confirmed by the calculated $\Delta G°$ values which occurred negative. So, by applying the linearized form of the Van't Hoff equation (**Equation 6**) to $\ln(K_{eq})$ versus 1/T

(**Figure 5C**), the values of $\Delta H°_{298}$ and $\Delta S°_{298}$ were also inferred (**Table S3**). As expected, $\Delta H°_{298} > 0$ (+17 KJ/mol) corroborated the endothermicity of the process, while $\Delta S°_{298} > 0$ (+100 J/mol×K) indicated the randomness of the interactions at the adsorbent–adsorbate interface, as previously observed in similar works.[16] Moreover, the small value of $\Delta H°_{298}$ (< 40 kJ/mol) reflected the involvement of weak and physical forces in the adsorption process.[18]

3.6 Isotherms of adsorption. Figure 6 reports the results obtained by applying the linearized forms of Langmuir, Freundlich, Temkin, and Dubinin-Radushkevitch (D-R) isotherm models (**Equations 7-12**). After the linear fitting and the analysis of the corresponding R^2 values (**Table S4**), the applicability of all the isotherms, with exception of the Langmuir model, could be considered, and **Table S4** reports the corresponding calculated isotherm parameters.[11] These findings suggested that the adsorption cannot be described with a single mathematical model, highlighting the heterogeneous character of the process, as already observed in previous works.[2,9,11] In other words, the adsorption of Ciprofloxacin took place onto a heterogeneous surface and the adsorbent–adsorbate interactions affected the surface coverage, provoking changes of the heat of adsorption during the process. More information were obtained by considering the value of the *n* parameter (see **Table S4**), inferred from the Freundlich equation, and representing the adsorption strength. Values of 1/*n* included between 0 and 1, like those measured during this work, confirm that the adsorption process is favored.[11] The D-R model also fitted the experimental data, and the corresponding parameters were calculated (**Table S4**). The q_{max} experimentally obtained (2 mg/g) well agree with the Q_0 values. The involvement of the physisorption in the adsorption process was suggested by considering the small value of E calculated. In fact, an E = 2 KJ/mol, being less than 8 KJ/mol, confirmed the hypotheses and it was consistent with the calculated $\Delta H°_{298}$ value, as explained by previous literature.[18]

3.7 Effect of pH. To obtain information about the nature of the interaction between CIP and nanosponges, the pH effect on the adsorption process was investigated. CIP solutions, 5 mg/L, with pH values ranging from 2 to 12 were prepared by adding HCl or NaOH according to the case and put in contact with 0.25 g of adsorbent. As reported in **Figures 7A** and **7B**, the % of adsorbed CIP onto nanosponges and the corresponding q_t values were maxima at pH 6 and tended to decrease lowering and increasing the pH values (see also the *inset* in **Figure 7C**, in which, for the sake of comparison, the CIP % of adsorption, at 60 minutes, are reported at several pH values). At pH 2 and 12, the adsorption process was completely inhibited. As already evidenced in a similar study involving a Cyclodextrin based polymer,[18] the adsorption is clearly pH-dependent, revealing the main presence of CIP/nanosponges electrostatic interactions. However, to better understand this finding, the CIP molecular features and the PZC of nanosponges should be considered.

In general, the PZC is a concept correlated to the adsorption phenomenon, describing the condition in which the density of the electrical charge onto the surface of the adsorbent material is zero, and, considering the presence of the electric double layer around the charged surface, the diffuse ion layer fades away. pH_{PZC} does not express the absence of charges onto the adsorbent surface, but rather that the number of positive and negative charges present is equal, so overall the material is electroneutral. Usually, this condition is evaluated in relation to the pH of an electrolyte, and it is assigned to a given substrate, and it is an important characteristic for selecting a substrate suitable for the treatment of contaminated systems.[36,37]

As reported in **Figure 7C**, the adsorbent shows a PZC at around pH 7 indicating that the adsorbent was positively and negatively charged below and up this pH value (pH_{PZC}), respectively.

CIP molecules, instead, in aqueous solutions, present two pK_a values: $pK_{a1}\approx6$ corresponds to the deprotonation of the CIP carboxylic acid group, while $pK_{a2}\approx8$ regards the amine group protonation in the piperazine moiety (see **Figure 3**).[18,25,38] Indeed, CIP can be found as a cation (CIP^+) at pH lower than pKa_1, zwitterion ($CIP^{\pm}$)

in the range of pH between pK_{a1} and pK_{a2}, or anion (CIP^-) for pH greater than pKa_2.[39] So, different CIP species, exhibiting different affinity towards the adsorbent, can be present in water solution by changing the pH. On this basis, the results reported in **Figures 7A** and **7B** can be better understood. In the pH range 2-6, the protonation of the amino groups in water made the pollutant positively charged (CIP^+), then a repulsion arises between the pollutant and the positively charged adsorbent (**Scheme 1A**). Therefore, by decreasing the pH values, the % of CIP adsorption reduced, becoming completely inhibited under conditions of strong acidity. Furthermore, Yu *et al.*[18] suggested that pH=2 could affect also the adsorbent chemical stability hindering the CIP removal. Indeed, if the adsorbent was left in acid solutions for 24h, it seemed to be dissolved. Around pH 6, the pollutant started the carboxylic acid deprotonation and it occurred as a zwitterion, exhibiting both protonated amino groups and negatively charged carboxylic moieties. In particular, these latter groups favored the electrostatic interaction between CIP and the positively charged surface of the nanosponges, as already observed by Yu *et al.*,[18] further enhanced by less important interactions involving H-bonds, the C=O coordination of CIP, and host-guest type hydrophobic interaction between Cyclodextrins and CIP.[18,40] At pH 8, the deprotonation of CIP amino groups occurred, therefore the presence of the carboxylic moieties rendered the molecules negatively charged; at the same time the polymer acquired a negatively charged surface repelling CIP^- and thus the process resulted slowed down, but not inhibited. This could be interpreted considering that, although the solution pH was alkaline (pH 8 and 10) and the amino group deprotonation occurred, probably there will be still some positively charged amino groups able to electrostatically interact with the negatively charged surface of the nanosponges. Instead, at pH 12, where both adsorbent and adsorbate were completely negatively charged, the adsorption process was completely inhibited.

3.8 Effect of salts in CIP solutions. Experiments of adsorption were performed by evaluating the ionic strength effect on the process to better evidence the key role of electrostatic interaction between CIP and CDs-based nanosponges.[9,16,18,34] In fact, the ionic strength can affect the adsorption

process playing two roles: the salting-out and competition effect. The first essentially regards the solubility of adsorbent and adsorbate that could be modified by the presence of inorganic electrolytes in the solution, with an effect also on the adsorbent performances. About the competition influence, by changing the ionic strength by adding inorganic salts, these latter could compete with adsorbate molecules for the adsorbent active sites. Therefore, the ionic strength could affect the adsorption capacity.

For this purpose, NaCl was selected as an electrolyte model, and different concentrations were studied calculating the % of CIP adsorption and the corresponding q_t values (**Figures 8A** and **8B**). In particular, the experiments were performed, once again, by adopting pH=6, corresponding to the maximum removal condition of the CIP, 5 mg/L as pollutant concentration, and 0.25 g of adsorbent, that was positively charged under this condition of work (pH_{PZC}=7). As can be observed in **Figures 8A** and **8B**, by increasing the salt concentration from 0.625×10^{-3} M to 0.1 M, the pollutant removal, and thus the q_t values, decreased with the complete lack of adsorption in presence of NaCl concentration greater than 0.01 M. This behavior was already observed in similar works[9,18,35] and particularly, considering the CIP, the work of Yu *et al.*[18] suggested that negative ions, Cl^- in this case, can compete with the adsorbate for the active adsorption sites on the adsorbent due to the positively charged adsorbent surface at pH 6 (**Scheme 1B**). Also if in presence of a different adsorbent, Khan *et al.*[16] obtained the same results and confirmed how the adsorption process mainly involved electrostatic interactions between CIP and the adsorbent surface.

At the same time, the CIP coordination ability toward ions should be also taken into consideration to further explain the observed results.[9] Indeed, to infer more information, the effect on the process of both anions and cations typologies was investigated. By choosing 5×10^{-3} M as salt concentration, the electrolyte type was changed by maintaining constant the anion (Cl^-) and changing the cation, analyzing the series: Li^+, Na^+, K^+, Mg^{2+}, and Ca^{2+}. The experimental results are reported in **Figures 8C** and **8D**. As it is possible to observe, the CIP removal percentage and the related q_t decreased by increasing the cation size, from Li^+ to K^+. Besides, by changing the cation charge, passing from

monovalent to divalent cations, by using Ca^{2+} and Mg^{2+}, this effect was more pronounced, and, in particular, a complete block of the adsorption was observed in presence of $MgCl_2$. These data confirmed the presence of interactions between the functional groups, *i.e.* the carboxylic acid group, the N-heterocycle in the piperazinyl ring, and carbonyl oxygen atom (see **Figure 3**), of CIP and the cations in the solution that slow down the adsorption process by shielding the CIP carboxylic negative charge, hindering the interaction between the contaminant and the nanosponges (**Scheme 1B**).[9,11] The shielding effect was more evident in the case of divalent cations compared to the monovalent ones. This behavior could be interpreted considering that, thanks to its chemical functionalities, the pollutant can coordinate metal ions forming complexes having different stoichiometry and stability.[31,41,42] In particular, according to Aristilde *et al.*,[43] nonetheless the interaction with calcium ion favors a 1:2 complex with CIP, more stable than the one with Mg^{2+}, the smaller binding length calculated for the Mg^{2+}-carboxylate adduct indicates a stronger binding of Mg^{2+} to the CIP molecules. This may justify the lack of adsorption of the CIP in presence of $MgCl_2$. So, the strong complexation ability of CIP with Ca^{2+} and Mg^{2+} in solution further inhibited its adsorption, especially when Mg^{2+} was in use, and the results highlighted the involvement, during the adsorption, of the suggested CIP functional groups (the carboxylic acid function and the carbonyl oxygen atom). Probably Ca^{2+} can act as a bridge between the CIP functional groups and adsorbent favoring the adsorption if compared with Mg^{2+}.[44] Indeed, due to the reduced size of Mg^{2+}, more coordinated complexes between CIP and this ion should be less favored with respect Ca^{2+}.[45] Only if the concentration of $MgCl_2$ and $CaCl_2$ was decreased to 0.6×10^{-3} M, a CIP slower adsorption was obtained with efficiencies, after 30 minutes of contact time, of 45 and 55%, respectively. Overall, the salt effect related to its concentrations was, for all the discussed salts, the same as those observed when NaCl was used; as a whole, the results corroborated the main involvement, during the process, of electrostatic interaction.[23] To further confirm the main involvement of Coulombian forces, the nature of anions was also changed;[9] in particular, selecting Na^+ as a cation, the results reported in **Figures 8E** and **8F** and related to NaCl, NaBr, $NaNO_3$, and $NaClO_4$, were obtained: by increasing the

size of the anion, *i.e.* Cl^-, Br^-, NO_3^- and ClO_4^-, the % of adsorption and the corresponding q_t values were affected, as already observed during the change of the cations, indicating the shielding of the positively charged adsorbent by anions (**Scheme 1B**). So, the ionic strength effect was observed in terms of both the interaction between CIP and cations in solution and competition between anions for the adsorbent free sites.

3.9 Desorption of CIP and adsorbent recycling. Desorption experiments were also carried out to attest the recycling of the adsorbent and adsorbate. Indeed, this is a challenge for researchers that work in this filed, as arise from some works reported in **Table 1**.

In particular, interesting are the results described in references 12, 16 and in the range from 23 to 26, in which the regeneration of the adsorbent was considered. By using a graphene oxide-based material, a very high adsorption capacity (q_{max}=1826.64 mg/g) was found by Khan *et al.*[16] However, the adsorbent regeneration and reusability were investigated by using an HCl/ethanol mixture (with a 1:10 ratio). Lu *et al.*[12] assessed the CIP removal and desorption by using diamine-functionalized MCM-41; a q_{max} of 139.25 mg/g was obtained. In this case, the CIP release was observed by using a very acidic solution (pH 3), obtaining 70% of CIP desorption; the same was observed in presence of a very concentrated NaCl solution (3M). Magnetic biosorbents were studied by Zheng *et al.*[23] showing a q_{max}=527.93 mg/g. In this case, the regeneration of CIP-loaded adsorbents was investigated by using acetone, ethanol, 0.1M HCl, and a mixture of ethanol and HCl, inferring that only the ethanol/HCl mixture or 0.1 M of HCl were suitable for CIP desorption from the adsorbent.[23] Nodeh *et al.*[24] reported an adsorbent based on a nanocomposite of polyaniline and magnetic graphene oxide: a q_{max} of 106.38 mg/g was showed, obtaining the CIP release by using methanol.[24] A Zeolitic imidazolate framework-8 derived nanoporous carbon was proposed by Li *et al.*[25] (q_{max}=416.7 mg/L) with the possibility to desorb CIP by using ultrasound, for 5 min, and methanol (containing 10% ammonia).[25] It is worth mentioning that only two interesting works (**Table 1**) reported the use of Cyclodextrins-based adsorbents. For example, the polymer obtained by

β-Cyclodextrin (β-CD) cross-linked with EthyleneDiamine-Tetraacetic Acid (EDTA) exhibited a q_{max} of 448 mg/L.[18] However, in this study, the recycling of the material was not investigated. On the contrary, the Chitosan-EDTA-β-cyclodextrin based-polymer, studied by Zhao *et al*.,[26] showed a q_{max} of 47 mg/g and explores the possibility to regenerate it by using 1 M HNO_3 or 5% HCl in ethanol solution.[26]

On this ground, clearly arise that in the past, despite the high q_{max} values, not environmentally friendly approaches for the adsorbent regeneration were investigated. On the other hand in this work, due to the presence of mainly electrostatic interactions between CIP and nanosponges, the use of electrolyte solutions is proposed for mitigating the environmental impact proposing to regenerate the adsorbent a green approach important for real applications.

As previously described, since the salts reduced the CIP removal by hindering its adsorption, a key role in the CIP molecules desorption, after the adsorption, might be expected. Among salts, NaCl solutions were selected by exploring different concentrations. In particular, after the CIP (5 mg/L) adsorption on 0.25 g of adsorbent, by adopting a contact time of 60 minutes, the loaded adsorbent was placed, under continuous stirring, in contact with aqueous solutions of NaCl with concentrations in the range 0.5-0.05M. The % of CIP desorption was then calculated (**Figures 9A**), and the results suggested that by increasing the NaCl concentration to 0.1 or 0.5M, the % of the desorbed CIP increased. In particular, it was observed how the release was more pronounced and already complete after only 30 minutes of contact time. From **Figure 9A**, it is evident that the CIP release was NaCl dose-dependent: by reducing the electrolyte concentration, the CIP desorption decreased, and the process was not observed in presence of 5×10^{-3} M NaCl. On this basis, it is possible to assess that, by increasing the ionic strength of solutions containing the adsorbent, after the CIP adsorption, the ionic exchange can be favored inducing the CIP release, confirming the main presence of weak electrostatic forces.[9,18] So, with the aim to develop a sustainable procedure, according to Green Chemistry and Green Principles, a solution 0.1M NaCl was selected for the CIP recovery (by applying 30 minutes

as best time) and adsorbent reuse. For the purpose, several adsorption/desorption cycles were executed, by inferring, for each run, the % of the adsorbed/desorbed CIP reported in **Figure 9B**. In particular, the percentage of desorbed CIP was normalized for the corresponding adsorbed pollutant (by using 60 minutes as contact time) and washed with fresh water after each cycle, before putting it again in contact with fresh CIP solutions (5 mg/L) to start with the new consecutive cycle. However, although after several adsorption/desorption cycles, the desorption process remained very performant recovering 80% of the adsorbed CIP; the CIP adsorption slightly decreased after the 3rd cycle. In conclusion, these results, if compared with previous works, reported in **Table 1**, despite the obtained low q_t value (2 mg/g), pointed out the feasibility of lowering the process costs by extending the adsorbent lifetime and recovering CIP for greener technology.

3.10 Physicochemical features of the polymer after the CIP adsorption and desorption.

The features of the polymer after the CIP adsorption and desorption were investigated by using in synergy FTIR-ATR, TGA, DSC, SEM and XRD analyses. In particular, as can be observed in **Figure 2A**, the FTIR-ATR features of the polymer, previously described, were retained both after the CIP adsorption (red line) and the polymer recycle, obtained with the 1st (blue line) and 5th cycle (green line) of desorption. The absence of significant changes in band position, shape and relative intensity were observed evidencing that the main polymer functional groups were retained also after its use and reuse. Accordingly, no change in the TG profile (**Figure 2B** and its *inset*) was observed after the CIP adsorption (red line). Otherwise, the desorption treatment with NaCl solutions, to recycle the polymer (blue and green lines), produced important changes in the thermal stability profile, particularly in the range of 250-450 °C where two decomposition processes appeared, having the maximum rate at about 290°C and 390°C, respectively (see **Figure 2B** and the *inset*). The findings were confirmed by DSC analyses (**Figure 2C**). Once again, after the CIP adsorption (red line), the DSC profile appeared the same of one observed previous the CIP adsorption (black line). On the other hand, confirming the TG results, after the 1st (blue line) and 5th cycle (green line) of desorption, the

DSC analysis showed significant changes observing the presence of an exothermic peak at about 290 ◦C and the presence of a peak at higher temperature. As a result, the separation between these two processes, associated with the decomposition of the cross-linker backbones at a lower temperature, and with the decomposition of cyclodextrins at a higher temperature, as already observed in the literature studying similar polymers, suggested that the salt treatment could induce modifications in the polymer chains arrangements [44]. However, these changes, as discussed so far, did not affect the morphology, XRD pattern and FTIR features of the adsorbent retaining its high adsorption capacity after the recycle (as evidenced in Fig. 9B); so, novel horizons in the use of this adsorbent to treat industrial water are opened demonstrating its lifetime extension.

3.11 Removal of other pollutants: To evidence the performance of the proposed adsorbent material, different emerging pollutants were studied. The processes were studied by adopting the UV-Vis spectroscopy as discussed for CIP. As can be observed in **Table 2**, drugs and pesticides, as Diclofenac, Carbendazim, Furosemide, and Sulfamethoxazole were successfully eliminated from the water, obtaining high efficiencies of adsorption under the experimental conditions of work reported in **Table 2**. Apart from Carbendazim, which, for being removed, needs a very long contact time (≈5h), all other substances were removed in a short time, *i.e.* 15 minutes. Unfortunately, the β-blocker Atenolol and the pesticide Propoxur were not removed. It is worth noting that the associated adsorption capacities q_{max} were also experimentally inferred for each emerging pollutant and the results are reported in **Table 2**.

Moreover, by selecting CIP, Diclofenac, Furosemide, and Sulfamethoxazole that were rapidly removed from the water, a quaternary mixture, containing each pollutant (5 mg/L), was prepared and 1 g of adsorbent was swelled inside. While **Figure S4A** reports the obtained results, **Figure S4B** shows the molecular structures of these pollutants. Each contaminant, as indicated in the *inset* of **Figure S4A**, shows a typical UV-Vis absorption spectrum that contributes to the UV-Vis absorption

spectrum of the mixture. In this case, an envelope of bands occurred due to the superposition of spectra ascribed to each EC. Overall, after 30 minutes of contact time with the adsorbent, the contribution of the pollutants disappeared in the spectrum (red curve **Figure S4A**), highlighting how the CIP was removed also in presence of other ECs that were also removed with high efficiency. So, the important absence of competition effects was denoted.

By considering these results, the proposed nanosponges should open a novel horizon in the environmental field because the same adsorbent is able, without the effect of competition, to remove a large number of pollutants belonging to different chemical families according to the challenge in this research field for real water treatments. A possible scale up, from laboratory to industrial scale is thus expected and work is in this direction in our laboratories.

4. CONCLUSIONS

This work reports the use of a Cyclodextrins based polymer for the EC removal from water. Diclofenac, Carbendazim, Furosemide, Ciprofloxacin, and Sulfamethoxazole were successfully eliminated from water obtaining high efficiencies of adsorption in a short time also if present in mixture. With the aim to give detailed information about the adsorption process, Ciprofloxacin was adopted as a model pollutant. Details about the adsorbent characterization were also presented by adopting in synergy different techniques such us FTIR-ATR, DSC, TG, SEM and XRD. The adsorption process was thermodynamically studied by changing temperature values, indicating that there is an increase in the pollutant removal from water by raising the temperature values. So, the process resulted to be spontaneous ($\Delta G°<0$), endothermic ($\Delta H°>0$), and with an increase of entropy. By using the isotherm and the kinetic models, it was observed how the adsorption process had a heterogeneous character, mainly involving physical interaction between CIP and the adsorbent. Indeed, Langmuir, Freundlich, Temkin, and Dubinin–Radushkevich were used to fit the experimental data. Furthermore, the pseudo-second-order kinetic model well described the adsorption process thus

indicating the kinetic relevance of the CIP adsorption on the adsorbent surface. Indeed, by increasing the polymer amount and diluting the Ciprofloxacin solution, the pollutant removal efficiency increased suggesting the important role of the adsorbent free active sites during the adsorption. The changes in pH values of solutions containing Ciprofloxacin played an important role in strengthening the presence of electrostatic interaction between the pollutant and the adsorbent. Indeed, the adsorption mainly occurred at pH 6 and it decreased both lowering or increasing the pH values in agreement with the pK_a values of the drug and the PZC (pH 7) of the adsorbent. The main presence of interaction between the carboxylic moiety of CIP and the positively charged polymer surface were suggested. In particular, the adsorption performed in presence of inorganic salts confirmed the finding slowing down the process. Not surprisingly, it is possible to induce the Ciprofloxacin desorption through a 0.1 M NaCl solution, exploiting an ionic exchange mechanism, and envisaging the recycling of both pollutants and adsorbent for several cycles, extending the lifetime of the adsorbent. In particular, the use of salt, to desorb the pollutant, affected the morphological and thermal features of the adsorbent, but it did not alter largely the polymer adsorption capacity favoring the Ciprofloxacin removal for several cycles of adsorption and desorption.

5. ACKNOWLEDGEMENTS.

We gratefully acknowledge Mr. Sergio Nuzzo for the skillful and technical assistance. This work was supported by the LIFE+ European Project named **LIFE CLEAN UP** ("Validation of adsorbent materials and advanced oxidation techniques to remove emerging pollutants in treated wastewater" [LIFE 16 ENV/ES/000169]. Adrián Matencio holds an aid to postdoctoral training and improvement abroad financed by the Consejería de Empleo, Universidades, Empresa y Medio Ambiente of the CARM, through the Fundación Séneca-Agencia de Ciencia y Tecnología de la Región de Murcia.

6. References

[1] V. Rizzi, J. Gubitosa, P. Fini, R. Romita, A. Agostiano, S. Nuzzo, P. Cosma, Commercial bentonite clay as low-cost and recyclable “natural” adsorbent for the Carbendazim removal/recover from water: Overview on the adsorption process and preliminary photodegradation considerations, Colloids Surfaces A Physicochem. Eng. Asp. (2020). https://doi.org/10.1016/j.colsurfa.2020.125060.

[2] V. Rizzi, J. Gubitosa, P. Fini, A. Petrella, R. Romita, A. Agostiano, P. Cosma, A “classic” material for capture and detoxification of emergent contaminants for water purification: The case of tetracycline, Environ. Technol. Innov. 19 (2020) 100812. https://doi.org/https://doi.org/10.1016/j.eti.2020.100812.

[3] V. Rizzi, E.A. Prasetyanto, P. Chen, J. Gubitosa, P. Fini, A. Agostiano, L. De Cola, P. Cosma, Amino grafted MCM-41 as highly efficient and reversible ecofriendly adsorbent material for the Direct Blue removal from wastewater, J. Mol. Liq. 273 (2019). https://doi.org/10.1016/j.molliq.2018.10.060.

[4] V. Rizzi, F. Fiorini, G. Lamanna, J. Gubitosa, E.A. Prasetyanto, P. Fini, F. Fanelli, A. Nacci, L. De Cola, P. Cosma, Polyamidoamine-Based Hydrogel for Removal of Blue and Red Dyes from Wastewater, Adv. Sustain. Syst. (2018). https://doi.org/10.1002/adsu.201700146.

[5] V. Rizzi, F. D’Agostino, P. Fini, P. Semeraro, P. Cosma, An interesting environmental friendly cleanup: The excellent potential of olive pomace for disperse blue adsorption/desorption from wastewater, Dye. Pigment. 140 (2017). https://doi.org/10.1016/j.dyepig.2017.01.069.

[6] V. Rizzi, A. Longo, T. Placido, P. Fini, J. Gubitosa, T. Sibillano, C. Giannini, P. Semeraro, E. Franco, M. Ferrandiz, P. Cosma, A comprehensive investigation of dye–chitosan blended films for green chemistry applications, J. Appl. Polym. Sci. 135 (2018).

https://doi.org/10.1002/app.45945.

[7] P. Semeraro, V. Rizzi, P. Fini, S. Matera, P. Cosma, E. Franco, R. Garc?a, M. Ferr?ndiz, E. N??ez, J.A. Gabald?n, I. Fortea, E. P?rez, M. Ferr?ndiz, Interaction between industrial textile dyes and cyclodextrins, Dye. Pigment. 119 (2015). https://doi.org/10.1016/j.dyepig.2015.03.012.

[8] A. Petrella, D. Spasiano, V. Rizzi, P. Cosma, M. Race, N. De Vietro, N. De Vietro, Lead Ion Sorption by Perlite and Reuse of the Exhausted Material in the Construction Field, Appl. Sci. 8 (2018) 1882. https://doi.org/10.3390/app8101882.

[9] V. Rizzi, J. Gubitosa, P. FINI, R. Romita, S. Nuzzo, P. Cosma, Chitosan Biopolymer from Crab Shell as Recyclable Film to Remove/Recover in Batch Ketoprofen from Water: Understanding the Factors Affecting the Adsorption Process, Materials (Basel). 12 (2019) 3810. https://doi.org/10.3390/ma12233810.

[10] V. Rizzi, F. Romanazzi, J. Gubitosa, P. Fini, R. Romita, A. Agostiano, A. Petrella, P. Cosma, Chitosan Film as Eco-Friendly and Recyclable Bio-Adsorbent to Remove/Recover Diclofenac, Ketoprofen, and their Mixture from Wastewater, Biomolecules. 9 (2019) 571. https://doi.org/10.3390/biom9100571.

[11] V. Rizzi, D. Lacalamita, J. Gubitosa, P. Fini, A. Petrella, R. Romita, A. Agostiano, J.A. Gabaldón, M.I. Fortea Gorbe, T. Gómez-Morte, P. Cosma, Removal of tetracycline from polluted water by chitosan-olive pomace adsorbing films, Sci. Total Environ. 693 (2019) 133620. https://doi.org/10.1016/j.scitotenv.2019.133620.

[12] D. Lu, S. Xu, W. Qiu, Y. Sun, X. Liu, J. Yang, J. Ma, Adsorption and desorption behaviors of antibiotic ciprofloxacin on functionalized spherical MCM-41 for water treatment, J. Clean. Prod. 264 (2020) 121644. https://doi.org/10.1016/j.jclepro.2020.121644.

[13] H. Fan, Y. Ma, J. Wan, Y. Wang, Z. Li, Y. Chen, Adsorption properties and mechanisms of

novel biomaterials from banyan aerial roots via simple modification for ciprofloxacin removal, Sci. Total Environ. 708 (2020) 134630. https://doi.org/10.1016/j.scitotenv.2019.134630.

[14] J. Ma, M. Yang, F. Yu, J. Zheng, Water-enhanced Removal of Ciprofloxacin from Water by Porous Graphene Hydrogel, Sci. Rep. 5 (2015) 13578. https://doi.org/10.1038/srep13578.

[15] A. Ashiq, B. Sarkar, N. Adassooriya, J. Walpita, A.U. Rajapaksha, Y.S. Ok, M. Vithanage, Sorption process of municipal solid waste biochar-montmorillonite composite for ciprofloxacin removal in aqueous media, Chemosphere. 236 (2019) 124384. https://doi.org/10.1016/j.chemosphere.2019.124384.

[16] N.A. Khan, T. Najam, S.S.A. Shah, E. Hussain, H. Ali, S. Hussain, A. Shaheen, K. Ahmad, M. Ashfaq, Development of Mn-PBA on GO sheets for adsorptive removal of ciprofloxacin from water: Kinetics, isothermal, thermodynamic and mechanistic studies, Mater. Chem. Phys. 245 (2020) 122737. https://doi.org/10.1016/j.matchemphys.2020.122737.

[17] T. Van Tran, D.T.C. Nguyen, H.T.N. Le, T.T.K. Tu, N.D. Le, K.T. Lim, L.G. Bach, T.D. Nguyen, MIL-53 (Fe)-directed synthesis of hierarchically mesoporous carbon and its utilization for ciprofloxacin antibiotic remediation, J. Environ. Chem. Eng. 7 (2019) 102881. https://doi.org/10.1016/j.jece.2019.102881.

[18] F. Yu, D. Chen, J. Ma, Adsorptive removal of ciprofloxacin by ethylene diaminetetraacetic acid/β-cyclodextrin composite from aqueous solution, New J. Chem. 42 (2018) 2216–2223. https://doi.org/10.1039/C7NJ03770H.

[19] M.Z. Afzal, X.-F. Sun, J. Liu, C. Song, S.-G. Wang, A. Javed, Enhancement of ciprofloxacin sorption on chitosan/biochar hydrogel beads, Sci. Total Environ. 639 (2018) 560–569. https://doi.org/10.1016/j.scitotenv.2018.05.129.

[20] H. Zhang, S.K. Khanal, Y. Jia, S. Song, H. Lu, Fundamental insights into ciprofloxacin

adsorption by sulfate-reducing bacteria sludge: Mechanisms and thermodynamics, Chem. Eng. J. 378 (2019) 122103. https://doi.org/10.1016/j.cej.2019.122103.

[21] L. Wang, C. Yang, A. Lu, S. Liu, Y. Pei, X. Luo, An easy and unique design strategy for insoluble humic acid/cellulose nanocomposite beads with highly enhanced adsorption performance of low concentration ciprofloxacin in water, Bioresour. Technol. 302 (2020) 122812. https://doi.org/10.1016/j.biortech.2020.122812.

[22] M.Y. Nassar, I.S. Ahmed, M.A. Raya, A facile and tunable approach for synthesis of pure silica nanostructures from rice husk for the removal of ciprofloxacin drug from polluted aqueous solutions, J. Mol. Liq. 282 (2019) 251–263. https://doi.org/10.1016/j.molliq.2019.03.017.

[23] C. Zheng, H. Zheng, C. Hu, Y. Wang, Y. Wang, C. Zhao, W. Ding, Q. Sun, Structural design of magnetic biosorbents for the removal of ciprofloxacin from water, Bioresour. Technol. 296 (2020) 122288. https://doi.org/10.1016/j.biortech.2019.122288.

[24] M.K. Mohammadi Nodeh, S. Soltani, S. Shahabuddin, H. Rashidi Nodeh, H. Sereshti, Equilibrium, Kinetic and Thermodynamic Study of Magnetic Polyaniline/Graphene Oxide Based Nanocomposites for Ciprofloxacin Removal from Water, J. Inorg. Organomet. Polym. Mater. 28 (2018) 1226–1234. https://doi.org/10.1007/s10904-018-0782-2.

[25] S. Li, X. Zhang, Y. Huang, Zeolitic imidazolate framework-8 derived nanoporous carbon as an effective and recyclable adsorbent for removal of ciprofloxacin antibiotics from water, J. Hazard. Mater. 321 (2017) 711–719.

https://doi.org/10.1016/j.jhazmat.2016.09.065.

[26] F. Zhao, E. Repo, D. Yin, L. Chen, S. Kalliola, J. Tang, E. Iakovleva, K.C. Tam, M. Sillanpää, One-pot synthesis of trifunctional chitosan-EDTA-β-cyclodextrin polymer for simultaneous removal of metals and organic micropollutants, Sci. Rep. 7 (2017) 15811.

https://doi.org/10.1038/s41598-017-16222-7.

[27] R. Cavalli, F. Trotta, W. Tumiatti, Cyclodextrin-based Nanosponges for Drug Delivery, J. Incl. Phenom. Macrocycl. Chem. 56 (2006) 209–213. https://doi.org/10.1007/s10847-006-9085-2.

[28] I. Krabicová, S.L. Appleton, M. Tannous, G. Hoti, F. Caldera, A. Rubin Pedrazzo, C. Cecone, R. Cavalli, F. Trotta, History of Cyclodextrin Nanosponges, Polymers (Basel). 12 (2020) 1122. https://doi.org/10.3390/polym12051122.

[29] P. Shende, Y.A. Kulkarni, R.S. Gaud, K. Deshmukh, R. Cavalli, F. Trotta, F. Caldera, Acute and Repeated Dose Toxicity Studies of Different β-Cyclodextrin-Based Nanosponge Formulations, J. Pharm. Sci. 104 (2015) 1856–1863.

https://doi.org/10.1002/jps.24416.

[30] A. Matencio, M.A. Guerrero-Rubio, F. Caldera, C. Cecone, F. Trotta, F. García-Carmona, J.M. López-Nicolás, Lifespan extension in Caenorhabditis elegans by oxyresveratrol supplementation in hyper-branched cyclodextrin-based nanosponges, Int. J. Pharm. 589 (2020) 119862. https://doi.org/10.1016/j.ijpharm.2020.119862.

[31] C. Varan, A. Anceschi, S. Sevli, N. Bruni, L. Giraudo, E. Bilgiç, P. Korkusuz, A.B. İskit, F. Trotta, E. Bilensoy, Preparation and characterization of cyclodextrin nanosponges for organic toxic molecule removal, Int. J. Pharm. 585 (2020) 119485. https://doi.org/10.1016/j.ijpharm.2020.119485.

[32] N. Rajendiran, T. Mohandoss, J. Thulasidhasan, Encapsulation of ciprofloxacin, sparfloxacin, and ofloxacin drugs with α- and β-cyclodextrins: spectral and molecular modelling studies, Phys. Chem. Liq. 54 (2016) 193–212. https://doi.org/10.1080/00319104.2015.1074046.

[33] Y.X. Wang, H.H. Ngo, W.S. Guo, Preparation of a specific bamboo based activated carbon and its application for ciprofloxacin removal, Sci. Total Environ. 533 (2015) 32–39. https://doi.org/10.1016/j.scitotenv.2015.06.087.

[34] H. Chen, B. Gao, H. Li, Removal of sulfamethoxazole and ciprofloxacin from aqueous solutions by graphene oxide, J. Hazard. Mater. 282 (2015) 201–207. https://doi.org/10.1016/j.jhazmat.2014.03.063.

[35] F. Yu, S. Sun, S. Han, J. Zheng, J. Ma, Adsorption removal of ciprofloxacin by multi-walled carbon nanotubes with different oxygen contents from aqueous solutions, Chem. Eng. J. 285 (2016) 588–595. https://doi.org/10.1016/j.cej.2015.10.039.

[36] E.N. Bakatula, D. Richard, C.M. Neculita, G.J. Zagury, Determination of point of zero charge of natural organic materials, Environ. Sci. Pollut. Res. 25 (2018) 7823–7833. https://doi.org/10.1007/s11356-017-1115-7.

[37] J. Drzymala, Z. Sadowski, L. Holysz, E. Chibowski, Ice/Water Interface: Zeta Potential, Point of Zero Charge, and Hydrophobicity, J. Colloid Interface Sci. 220 (1999) 229–234. https://doi.org/10.1006/jcis.1999.6528.

[38] S. Xing, W. Li, B. Liu, Y. Wu, Y. Gao, Removal of ciprofloxacin by persulfate activation with CuO: A pH-dependent mechanism, Chem. Eng. J. 382 (2020) 122837.

https://doi.org/10.1016/j.cej.2019.122837.

[39] M.E. Roca Jalil, M. Baschini, K. Sapag, Removal of Ciprofloxacin from Aqueous Solutions Using Pillared Clays, Mater. (Basel, Switzerland). 10 (2017) 1345. https://doi.org/10.3390/ma10121345.

[40] J. Chao, D. Meng, J. Li, H. Xu, S. Huang, Preparation and study on the novel solid inclusion complex of ciprofloxacin with HP-β-cyclodextrin, Spectrochim. Acta Part A Mol. Biomol.

Spectrosc. 60 (2004) 729–734. https://doi.org/10.1016/S1386-1425(03)00284-1.

[41] V. Uivarosi, Metal complexes of quinolone antibiotics and their applications: an update, Molecules. 18 (2013) 11153–11197. https://doi.org/10.3390/molecules180911153.

[42] P. Drevenšek, I. Turel, N. Poklar Ulrih, Influence of copper(II) and magnesium(II) ions on the ciprofloxacin binding to DNA, J. Inorg. Biochem. 96 (2003) 407–415. https://doi.org/10.1016/S0162-0134(03)00179-X.

[43] L. Aristilde, G. Sposito, Molecular modeling of metal complexation by a fluoroquinolone antibiotic, Environ. Toxicol. Chem. 27 (2008) 2304–2310. https://doi.org/10.1897/08-059.1.

[44] J.A. González, J.G. Bafico, M.E. Villanueva, S.A. Giorgieri, G.J. Copello, Continuous flow adsorption of ciprofloxacin by using a nanostructured chitin/graphene oxide hybrid material, Carbohydr. Polym. 188 (2018) 213–220.

https://doi.org/10.1016/j.carbpol.2018.02.021.

[45] J. Al-Mustafa, Z.A. Taha, Thermodynamics of the complexation of ciprofloxacin with calcium and magnesium perchlorate, Thermochim. Acta. 521 (2011) 9–13. https://doi.org/10.1016/j.tca.2011.03.033.

E. A. Dil, M. Ghaedi, A. Asfaram, F. Mehrabi, F. Sadeghfar. Efficient adsorption of Azure B onto CNTs/Zn:ZnO@Ni2P-NCs from aqueous solution in the presence of ultrasound wave based on multivariate optimization, J. Ind.Eng.Chem. 74 (2019) 55-62.

https://doi.org/10.1016/j.jiec.2018.12.050

E. A. Dil, M. Ghaedi, A. Asfaram, F. Mehrabi, A. A. Bazrafshan, L. Tayebi. Synthesis and application of Ce-doped TiO2 nanoparticles loaded on activated carbon for ultrasound-assisted

adsorption of Basic Red 46 dye, Ultrason. Sonochem., 58 (2019) 104702
https://doi.org/ 10.1016/j.ultsonch.2019.104702

F.MehrabI, E. A.Dil. Investigate the ultrasound energy assisted adsorption mechanism of nickel(II) ions onto modified magnetic cobalt ferrite nanoparticles: Multivariate optimization, Ultrason. Sonochem 37 (2017)37-46.
https://doi.org/10.1016/j.ultsonch.2016.12.038.

E. A.Dil, M.Ghaedi, A. Asfaram, F. Mehrabi, A. A.Bazrafshan. Optimization of process parameters for determination of trace Hazardous dyes from industrial wastewaters based on nanostructures materials under ultrasound energy, Ultrason. Sonochem. 40 (2018) 238-248.
https://doi.org/10.1016/j.ultsonch.2017.07.022. Epub 2017 Jul 14.

E. A.Dil, M. Ghaedi, G. R. Ghezelbash, A. Asfaram, A. M. Ghaedic, F. Mehrabic. Modeling and optimization of Hg2+ ion biosorption by live yeast Yarrowia lipolytica 70562 from aqueous solutions under artificial neural network-genetic algorithm and response surface methodology: kinetic and equilibrium study , *RSC Adv.***,** 6 (2016) 54149-54161
https://doi.org/10.1039/C6RA11292G

7. Figure and Tables

Adsorbent	Maximum adsorption capacity Q_{max} mg/g	Reference
Nanocomposite beads	9.21-10.87	Wang *et al.* 2020 [21]
Graphene oxide-based adsorbent	1826.64	Khan *et al*. 2020 [16]
Diamine-functionalized MCM-41	139.25	Lu *et al.* 2020 [12]
Magnetic biosorbents	527.93	Zheng *et al.* 2020 [23]
Municipal solid waste biochar-montmorillonite composite	167.36	Ashiq *et al.* 2019 [15]
Sulfate-reducing bacteria sludge	7.642	Zhang *et al.* 2019 [20]
Polyaniline-magnetic graphene oxide nanocomposite	106.38	Nodeh *et al.* 2018 [24]
Ethylene diaminetetraacetic acid– β -cyclodextrin	448	Yu *et al.* 2018 [18]
Chitosan hydrogel beads	1.024	Afzal *et al.* 2018 [19]

Nanoporous carbon from Zeolitic imidazolate framework-8	416.7	Li *et al.* 2017 [25]
chitosan-EDTA-β-cyclodextrin polymer	47 mg/g	Zhao *et al.* 2017 [26]
Cyclodextrins nanosponges	**2**	**This work**

Table 1: The most interesting and recent articles for the removal of CIP from water

ECs	**ECs amount mg/L**	**Amount of polymer (g)**	**Volume (mL)**	**% Adsorption (Contact Time 15 min)**	**Maximum adsorption capacity q_{max}**
Diclofenac	15	1	15	90	15
Carbendazim	10	1	15	70 (increased to 90 % in 5h)	0.3
Furosemide	10	1	15	90	4.5
Atenolol	15	1	15	NO	//
Ciprofloxacin	10	1	15	90	2
Propoxur	20	1	15	NO	//

Sulfamethoxazole	10	1	15	90	13

Table 2: Tested emerging pollutants; the experimental conditions of work, the % of adsorption and adsorption capacities are indicated.

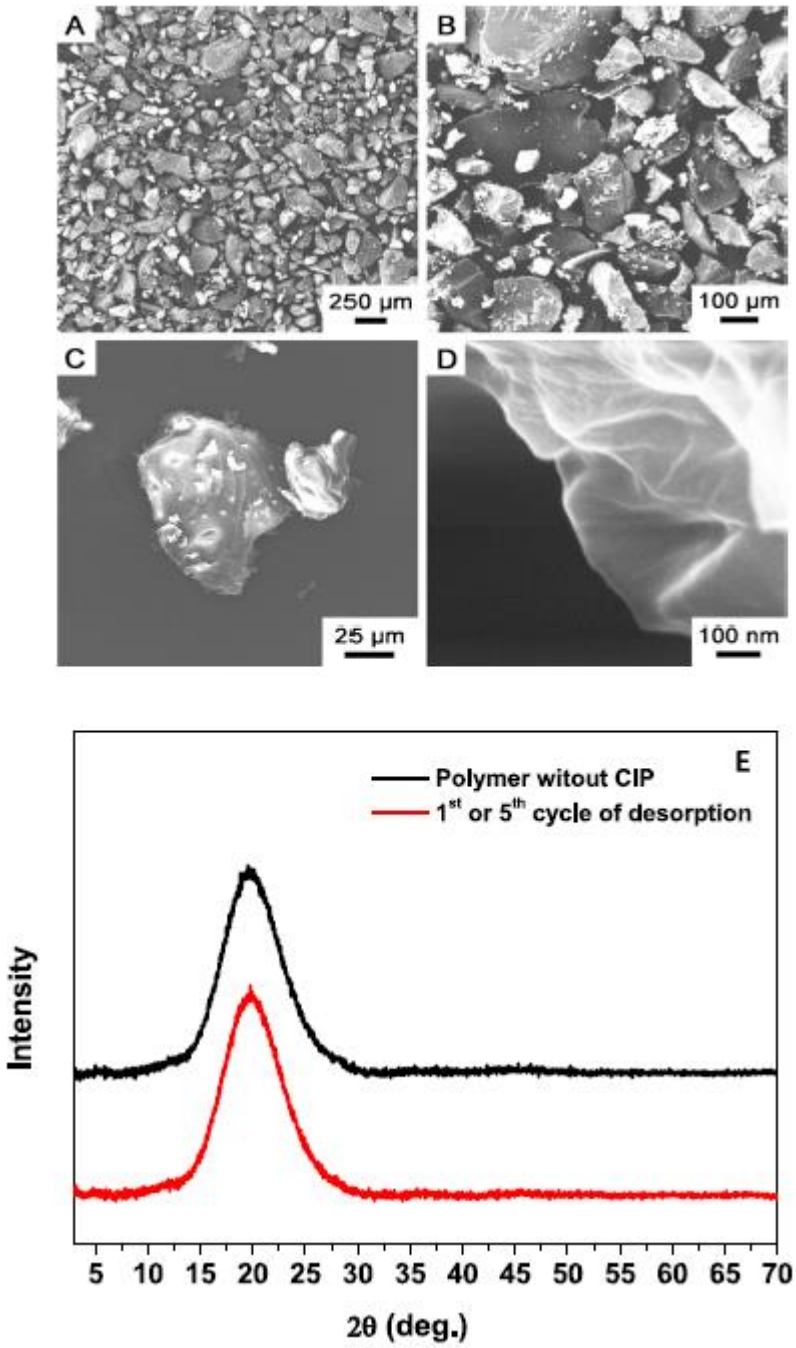

Figure 1: SEM (A) and XRD (A) analyses obtained for the adsorbent before and after the CIP adsorption. Furthermore, measurements after the 1st and 5th cycle of adsorption/desorption are reported. (nel caso ci sia XPS, se è possibile fare un pannello C.

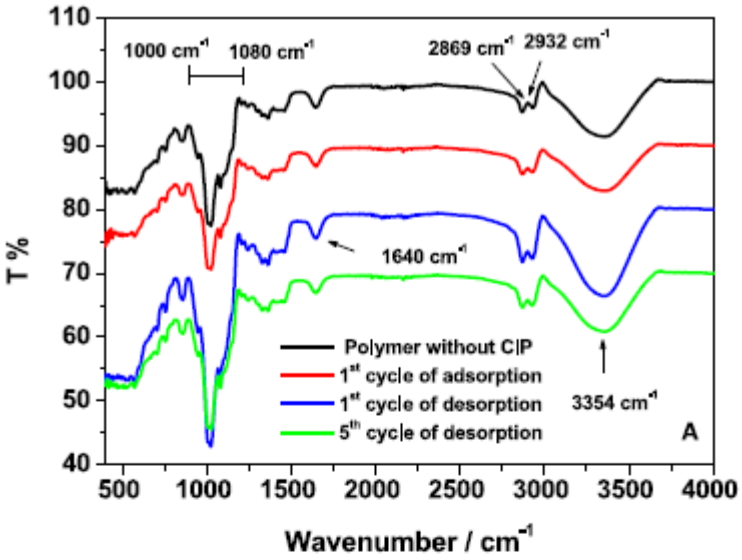
1000 cm-1
1080 cm-1
2869 cm-1
2932 cm-1
1640 cm-1
3354 cm-1
Polymer without CIP
1st cycle of adsorption
1st cycle of desorption
5th cycle of desorption
A
T %
Wavenumber / cm-1

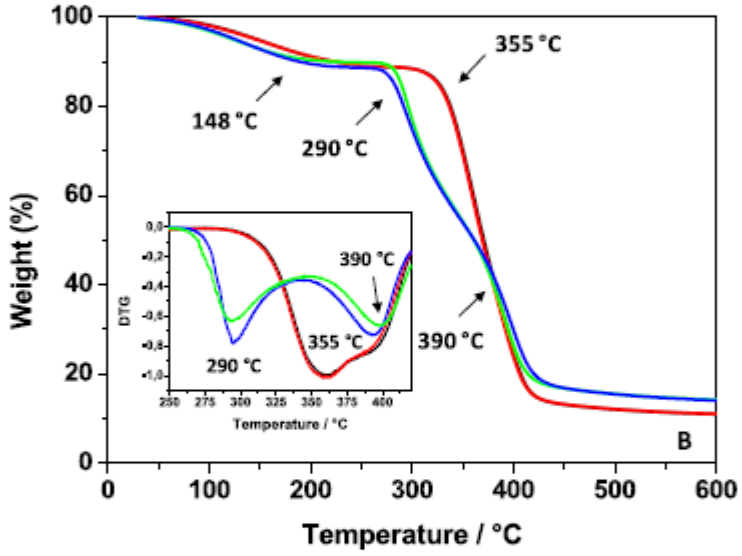
148 °C
290 °C
355 °C
390 °C
290 °C
355 °C
390 °C
DTG
Temperature / °C
B
Weight (%)
Temperature / °C

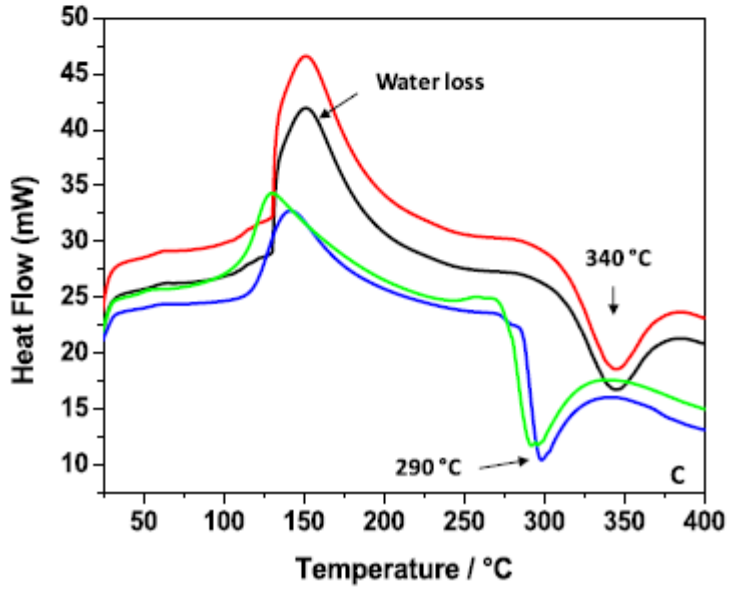
Water loss
340 °C
290 °C
C
Heat Flow (mW)
Temperature / °C

Figure 2: Comparison between FTIR-ATR spectra (wavenumbers range 450-4000 cm^{-1}) (A), TG (B) and DSC (C) analyses obtained for the adsorbent before and after the CIP adsorption. The inset reported in Figure 2B shows the DTG analysis focused in the temperature range 250-450 °C. Furthermore, measurements after the 1st and 5th cycle of adsorption/desorption are reported.

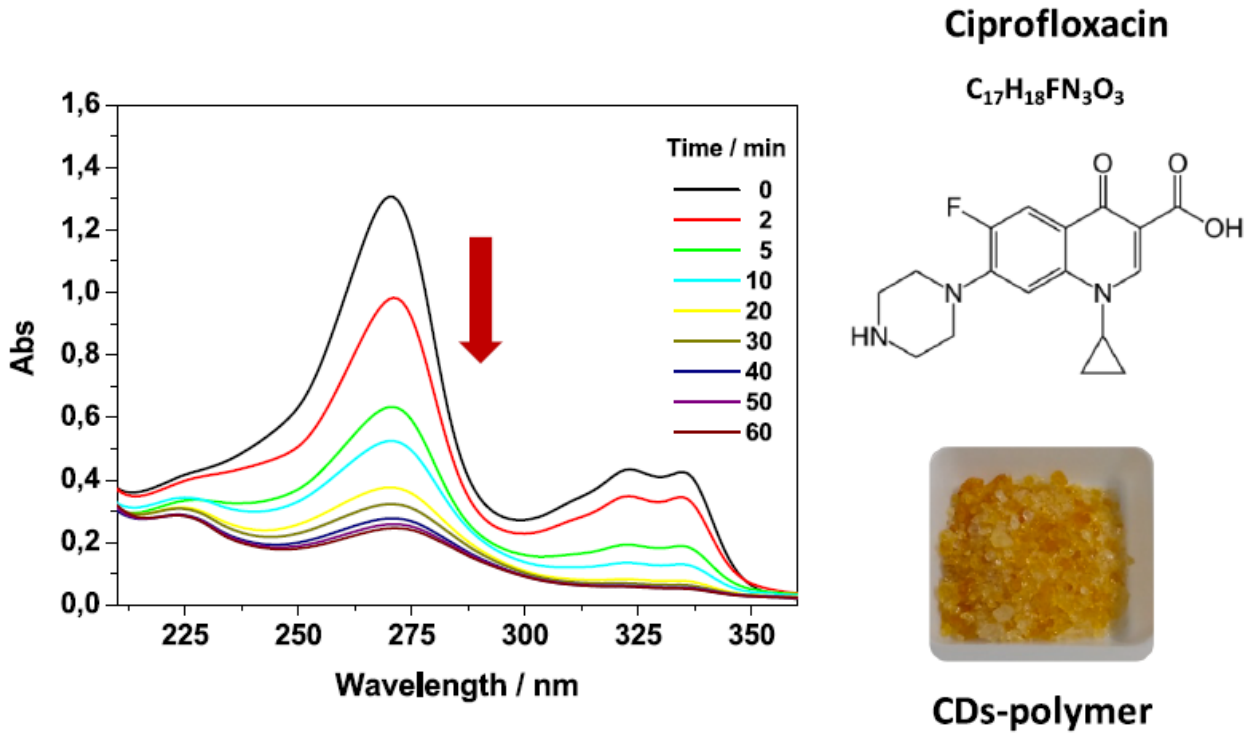

Figure 3: UV-Vis absorption spectra of a CIP solution, 10 mg/L, pH 6 at r.t., in presence of 1g of adsorbent, collected at several contact times; the chemical structure and formula of the pollutant and the adsorbent camera picture are also reported.

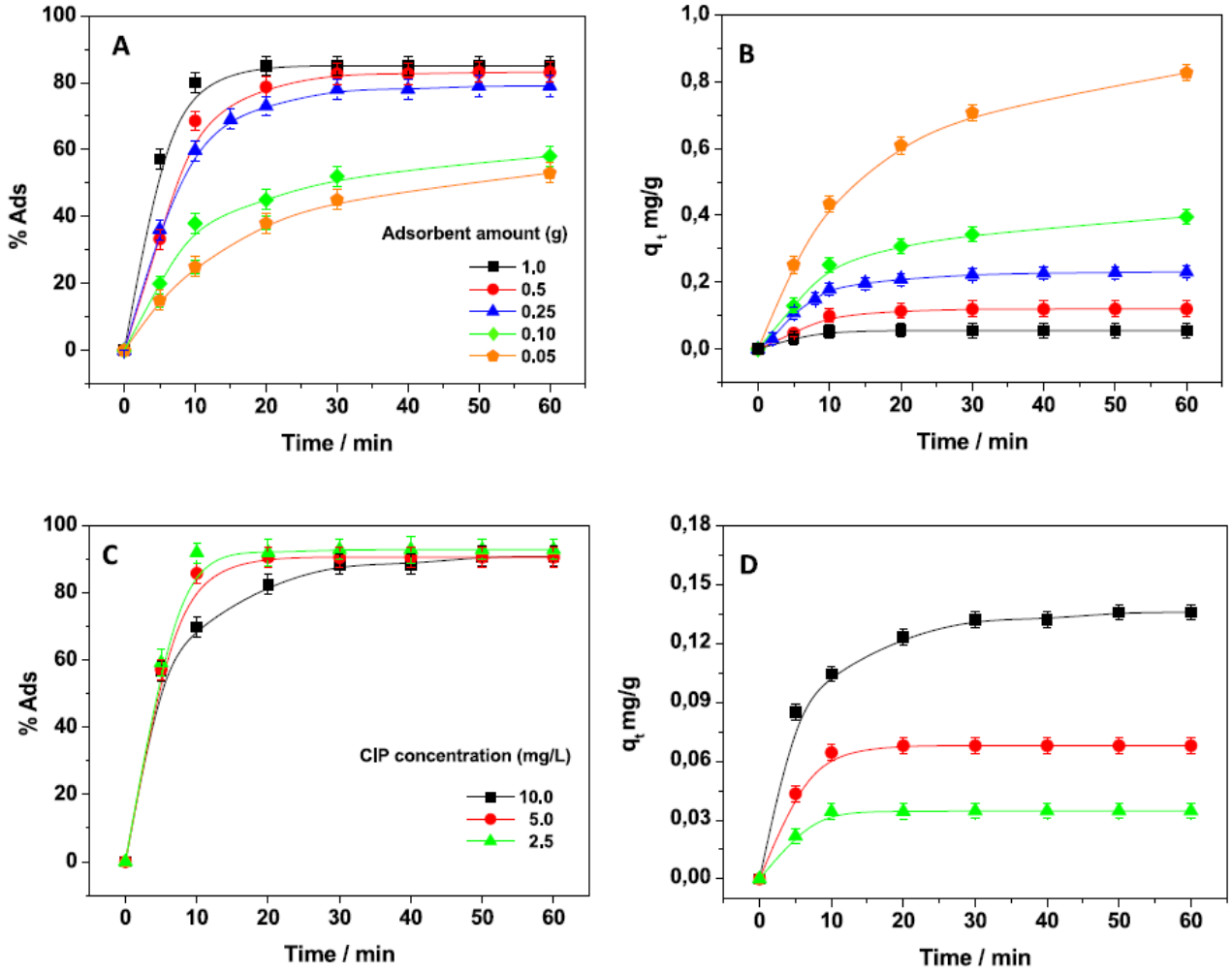

Figure 4: % of CIP adsorption onto nanosponges, with the corresponding adsorption capacities. (A, B) different adsorbent weights, [CIP] = 5 mg/L at pH 6 and r.t.; (C, D) different CIP concentrations, 2.5, 5 and 10 mg/L, at pH 6, by using 1 g of polymer.

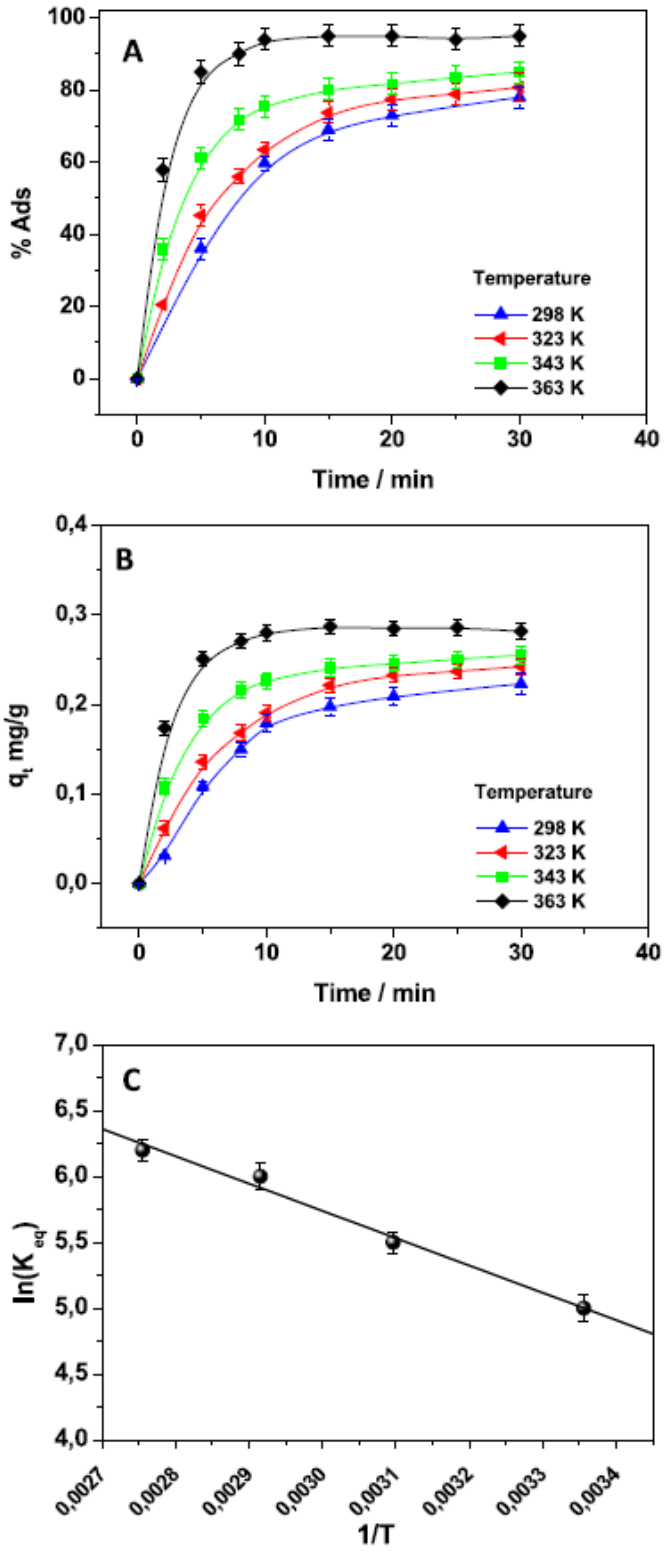

Figure 5: % of CIP adsorption (A) onto nanosponges (0.25g) with the related adsorption capacities (B) at several temperature values (from a CIP solution 5 mg/L, pH 6); Plot of ln(keq) vs 1/T to infer ΔH° and ΔS° at 298 K (C).

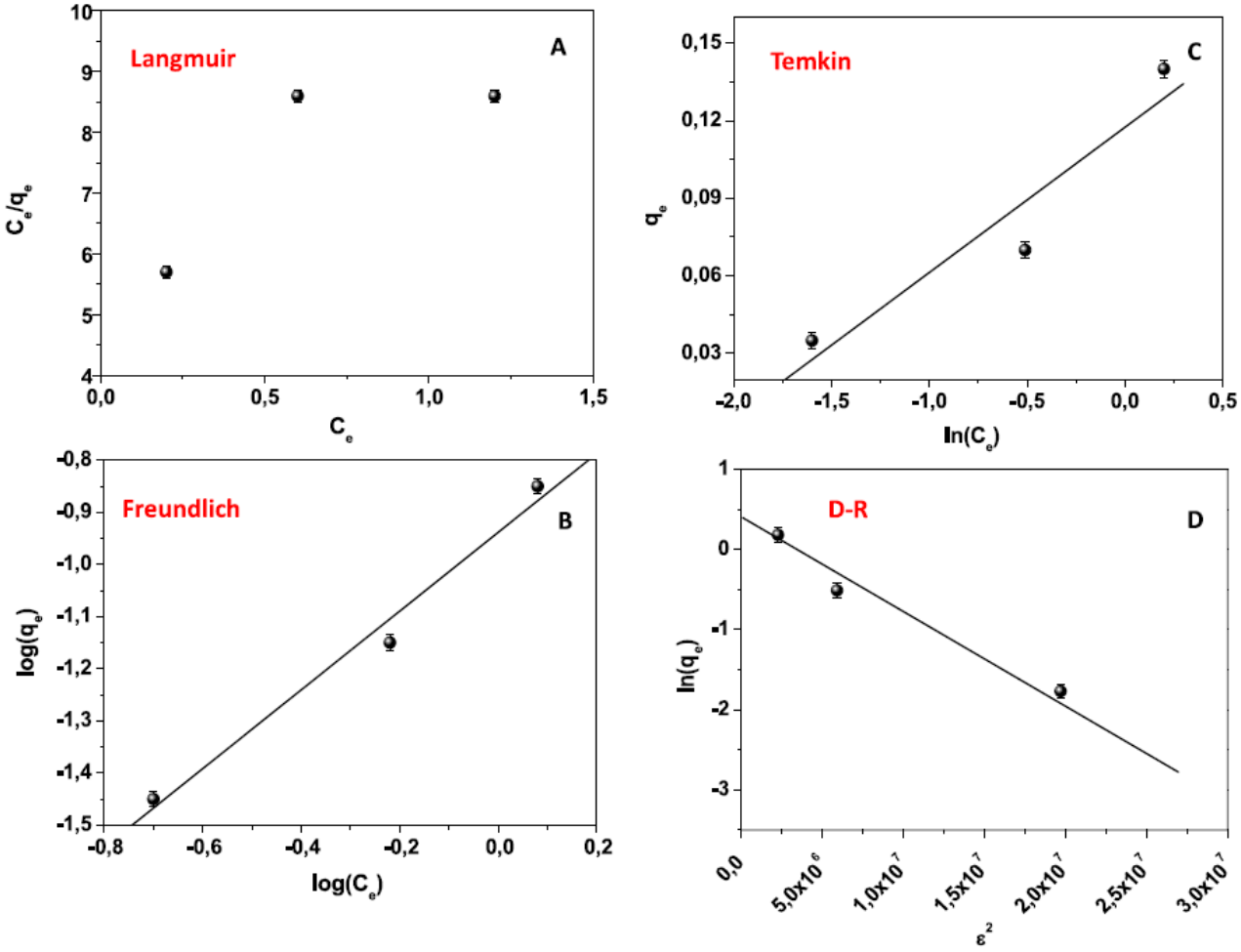

Figure 6: Isotherms of adsorption: (A) Langmuir, (B) Freundlich, (C) Temkin, and (D) D-R.

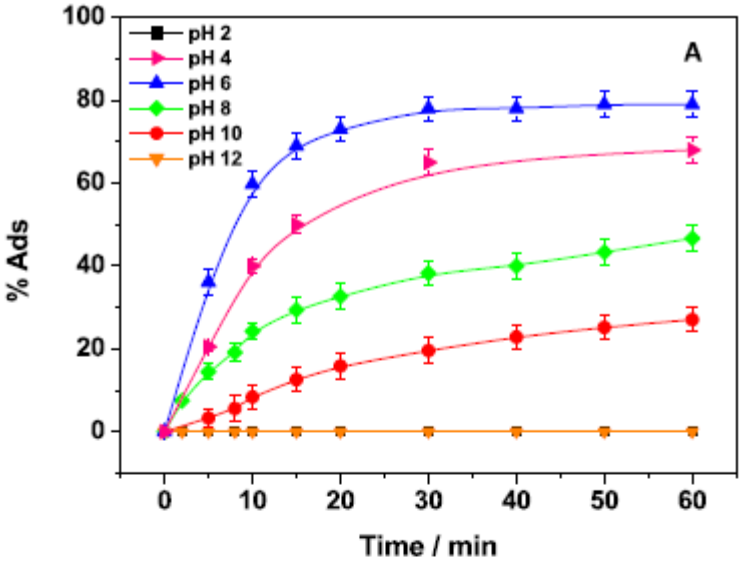
pH 2
pH 4
pH 6
pH 8
pH 10
pH 12
A
% Ads
Time / min

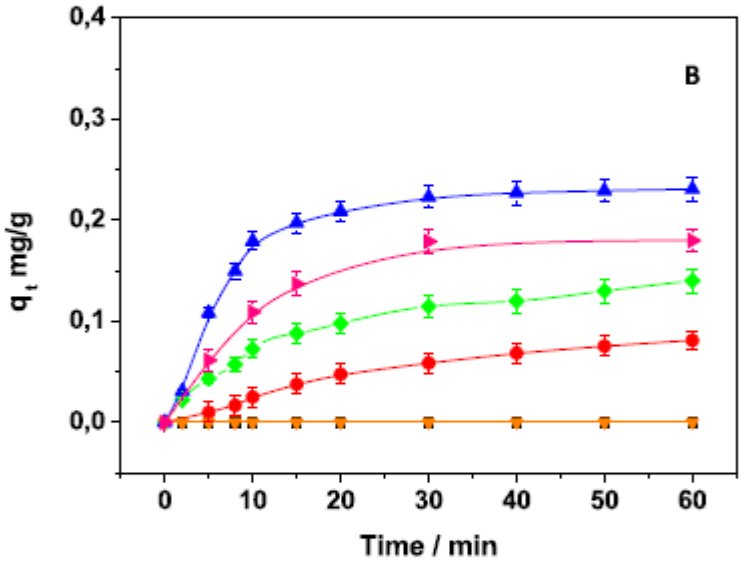
B
q_t mg/g
Time / min

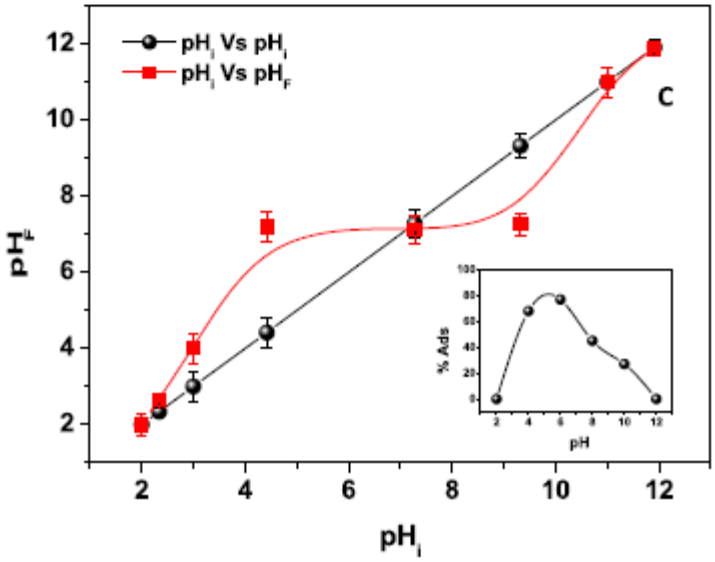
pH_i Vs pH_i
pH_i Vs pH_F
C
pH_F
pH_i
% Ads
pH

Figure 7: % of CIP adsorption (A) onto nanosponges (0.25g) with the related adsorption capacities (B) at several pH values (from a CIP solution 5 mg/L, pH 6); (C) application of the drift method to infer the adsorbent PZC; the inset reports the % of CIP adsorption, onto the adsorbent, at 60 minutes and at several pH values.

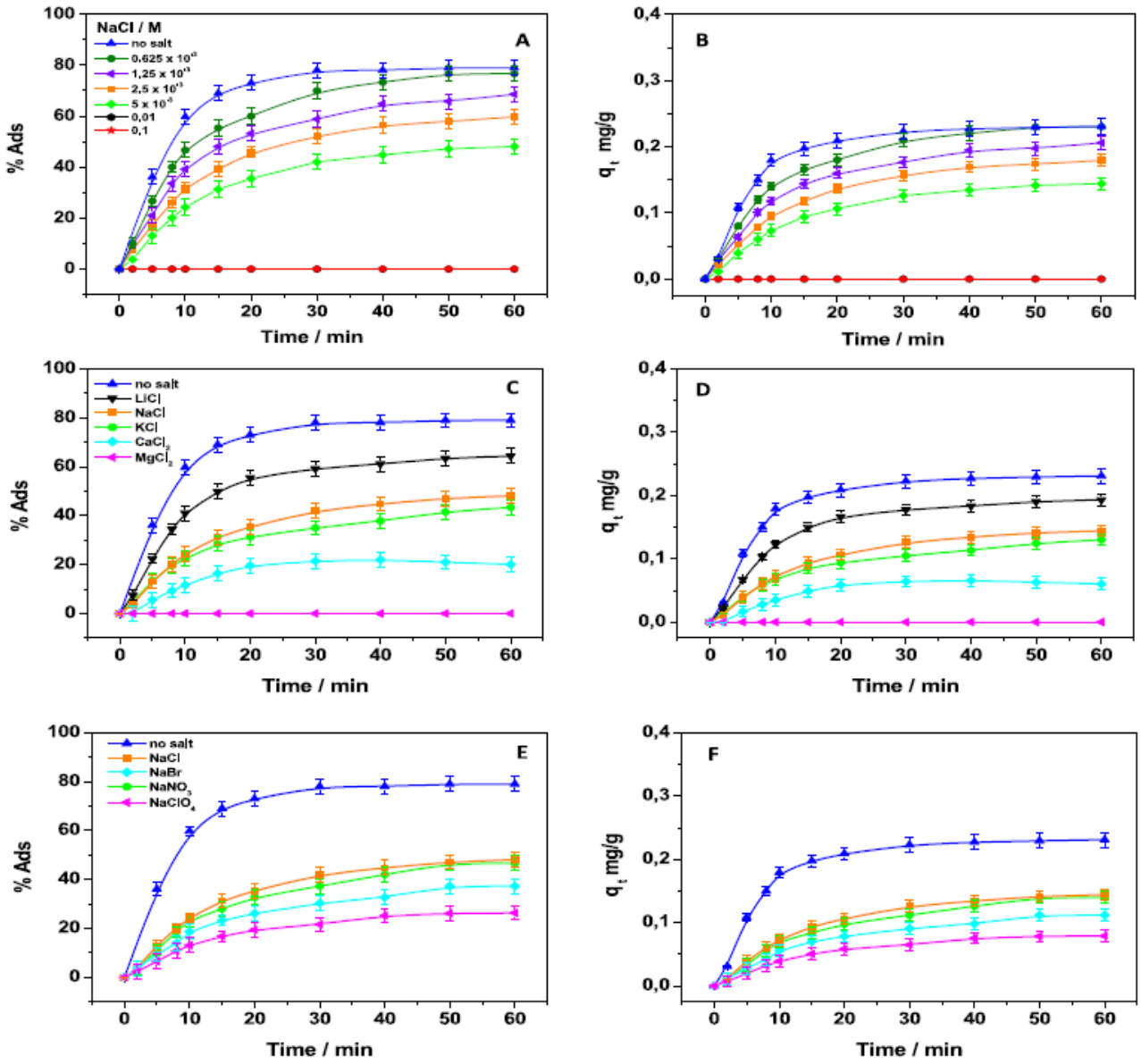

Figure 8: % of CIP adsorption (A) onto nanosponges with the related adsorption capacities (B) at several NaCl concentrations; % of CIP adsorption (C) onto nanosponges with the related adsorption capacities (D) by changing the cation nature (salt concentration:5 mM) and % of CIP adsorption (E) onto nanosponges with the related adsorption capacities (F) by changing the anion nature (salt

concentration: 5mM). All the experiments are related to a CIP solution 5 mg/L, pH 6 in presence of 0.25 g of adsorbent.

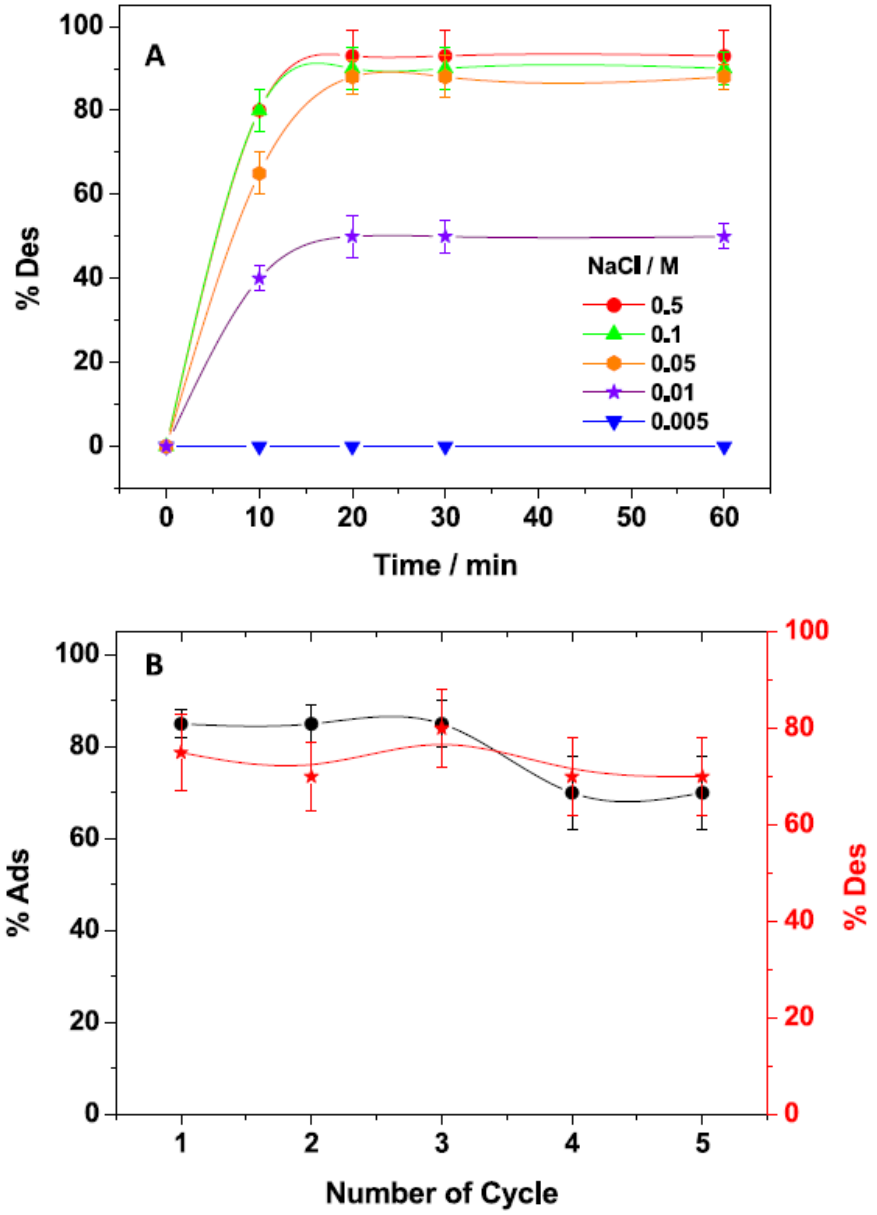

Figure 9: % of CIP desorption, in presence of different concentrations of NaCl, from nanosponges, and at several contact time (the related adsorption was obtained from a solution 5 mg/L by adopting 60 minutes as adsorption contact time and 0.25 g of adsorbent) (A); Consecutive cycles of CIP adsorption from a solution 5 mg/L (the contact time is 60 minutes, by adopting 1g of adsorbent) and

desorption in 0.1M NaCl (the % of desorption is calculated at 60 minutes adopted as contact time) (B).

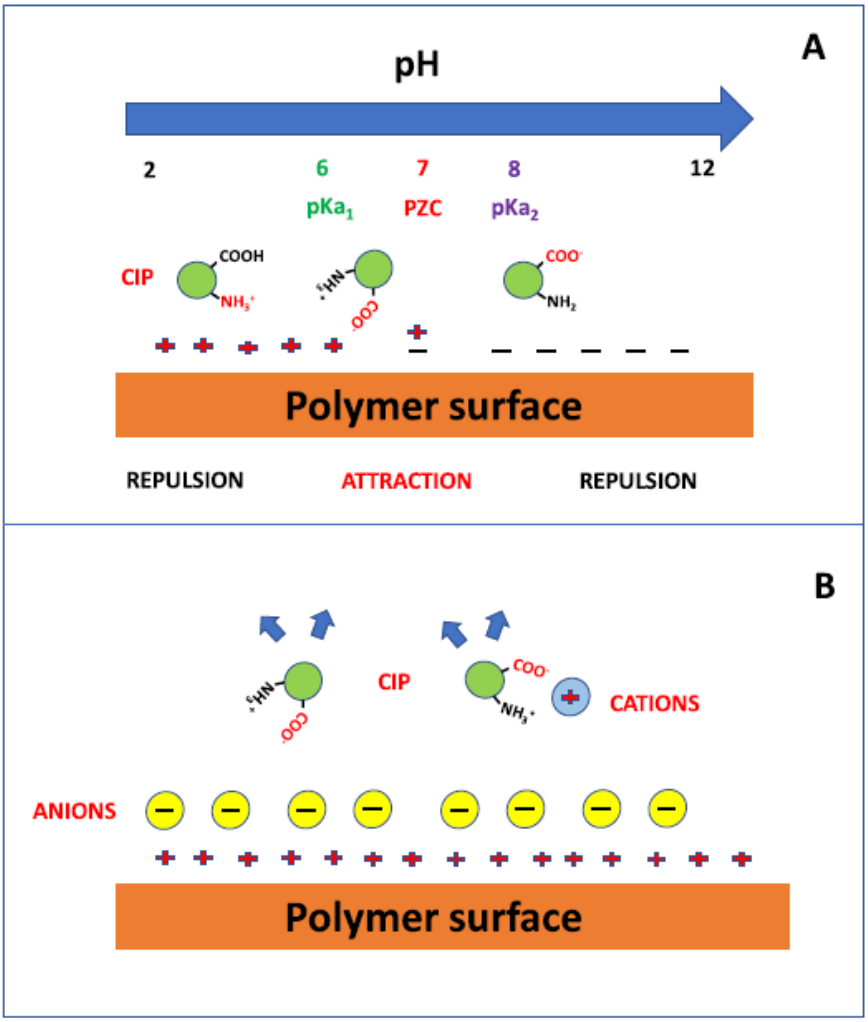

Scheme 1: Interaction between the adsorbent and CIP at several pH values (A) and in presence of anions/cations derived from salts (B).